J Nonlinear Sci (2017) 27:1829–1868
DOI 10.1007/s00332-017-9388-z

Journal of Nonlinear Science

Computation of Quasi-Periodic Normally Hyperbolic Invariant Tori: Algorithms, Numerical Explorations and Mechanisms of Breakdown

Marta Canadell[1] · **Àlex Haro**[2]

Received: 12 May 2016 / Accepted: 22 April 2017 / Published online: 8 May 2017

Abstract We present several algorithms for computing normally hyperbolic invariant tori carrying quasi-periodic motion of a fixed frequency in families of dynamical systems. The algorithms are based on a KAM scheme presented in Canadell and Haro (J Nonlinear Sci, 2016. doi:10.1007/s00332-017-9389-y), to find the parameterization of the torus with prescribed dynamics by detuning parameters of the model. The algorithms use different hyperbolicity and reducibility properties and, in particular, compute also the invariant bundles and Floquet transformations. We implement these methods in several 2-parameter families of dynamical systems, to compute quasi-periodic arcs, that is, the parameters for which 1D normally hyperbolic invariant tori with a given fixed frequency do exist. The implementation lets us to perform the continuations up to the tip of the quasi-periodic arcs, for which the invariant curves break down. Three different mechanisms of breakdown are analyzed, using several observables, leading to several conjectures.

Communicated by Eusebius Doedel.

M.C. and À.H. acknowledge support from the Spanish Grants MTM2012-32541 and MTM2015-67724-P, and the Catalan Grant 2014-SGR-1145. M.C. also acknowledges support from the FPI Grant BES-2010-039663, and the NSF Grant DMS-1500943.

✉ Àlex Haro
alex@maia.ub.es

Marta Canadell
marta_canadell@brown.edu

[1] ICERM, Brown University, 121 South Main street, Providence, RI 02903, USA

[2] Departament de Matemàtiques i Informàtica, Universitat de Barcelona, Gran Via 585, 08007 Barcelona, Spain

Keywords Normally hyperbolic invariant manifolds · KAM theory · Computational dynamical systems · Breakdown of invariant tori

Mathematics Subject Classification 37D10 · 37E45 · 37M99 · 65P99

1 Introduction

An important problem in dynamical systems and their applications in science and engineering is the existence of quasi-periodic oscillations, which are geometrically described as invariant tori. In applications, it is common to count with detuning parameters that the user can change to get the desired quasi-periodic response on the system at hand. Hence, having a method to select the detuning parameter and to compute the corresponding quasi-periodic response is very useful to control a system. Moreover, it is also important to develop algorithms of computation that let us continue with respect to internal (perturbation) parameters the external (detuning) parameters and the corresponding invariant torus, and study their range of validity. In particular, a phenomenon that is poorly understood is that of the breakdown of invariant tori, which is related with loss of reducibility properties. These are the objects of this paper.

Most algorithms that have been developed to this date to compute invariant tori consist in using Fourier approximations for the tori and solving the large systems of equations arising from the discretization of the invariance equations by using Newton's method. These *large matrix methods* were originally designed to study problems from celestial mechanics (Castellà and Jorba 2000; Jorba 2001), in the conservative context, and later were introduced in the dissipative context (Schilder et al. 2005). It was found that the practical use of taking frequencies as unknown could be the source of numerical instabilities when the resonances are strong enough. It was found that the practical use of taking frequencies as unknowns is capable to cross high-order resonances, but that low-order resonances are the source of numerical instabilities, since there is a strong dynamical obstruction to compute the torus with a rotational dynamics. An alternative is fixing the frequency and then adding the detuning parameter as unknown (Peckham and Schilder 2007; Vitolo et al. 2011). Even though these methods have been tested to be very efficient in many studies, we find two major problems. First, there are no rigorous results about the convergence of these schemes, from the point of view of numerical analysis. In fact, these methods have been developed rather independently of the fundamental results and methods of the so-called dissipative KAM theory (Moser 1966, 1967; Broer et al. 1996). We mention, however, the analysis of large matrices carried out in Bourgain (1997), to avoid the so-called second Melnikov condition for elliptic eigenvalues. Second, the range of applicability of large matrix methods is limited to cases in which the number of Fourier coefficients of the Fourier approximations is relatively small. Hence, these methods are hardly applicable for tori of dimension larger than 1, or in situations in which tori are about to break. Interestingly, Vitolo et al. (2011) encourages the development of alternatives to large matrix methods. Developing such alternative algorithms in the main purpose of this paper.

The development of methodologies that encompass both rigorous and numerical approaches is very appealing. This is perhaps the most important feature of the so-called *parameterization method* (Cabré et al. 2003; Haro et al. 2016), which is the conceptual framework of this paper. We derive several Newton-like methods of computation of normally hyperbolic invariant tori with a prescribed frequency in families of dynamical systems, in the dissipative context. The setting is described in Sect. 2. There is an underlying an a posteriori theorem that is presented in the companion paper Canadell and Haro (2016), which provides sufficient conditions for the convergence of a Newton-like method from an initial approximation. Such a theorem can lead to (computer-assisted) proofs of existence of invariant tori in specific problems, by checking its long list of hypotheses for an initial approximation, that could have been obtained by using the methods of this paper or by any other means (large matrix methods, perturbation theory, etc.). This step has not been pursued here, and we refer to Figueras et al. (2016) for computer-assisted proofs in the Hamiltonian context, specifically for Lagrangian invariant tori of exact symplectic maps. The computation of normally hyperbolic invariant tori with dynamics other than a rotation using the parameterization method is considered in Canadell (2014), Haro et al. (2016).

The algorithms are detailed in Sect. 3. The first algorithm is based on normal hyperbolicity, and computes the torus and the stable and unstable bundles, solving the linear equations arising from Newton's method by performing the corrections of the torus in the normal directions by projecting them onto the stable and unstable directions, while the detuning parameter is chosen in order to fix the corrections of the torus in the tangent directions. As such, this method shares some of the weaknesses of graph transform techniques, since the speed of convergence at each step of the Newton-like method is determined by the attraction and expansion rates in transverse directions to the torus. This problem can be mitigated by using fast iteration methods (Huguet et al. 2013; Canadell 2014). An alternative is using reducibility (to constant coefficients) whenever is possible (Haro and de la Llave 2006b, 2007; Jorba and Olmedo 2009) (see Haro et al. 2016 for some benchmarks comparing large matrix methods with reducibility methods). In such a case, the linear equations to be solved at each step of the Newton-like method are diagonalized in Fourier space, and then can be solved very efficiently. In particular, for discretizations with N Fourier modes, the memory storage is $O(N)$ and the computation time is $O(N \log N)$, while when using large matrix methods, the memory storage is $O(N^2)$ and the computation time is $O(N^3)$. Moreover, the algorithms based on reducibility let the continuation cross bifurcation parameters in which the torus changes stability properties.

The numerical explorations we present in this paper deal with continuation of one-dimensional tori with a fixed frequency ω (the golden mean) in several two-parameter families of dynamical systems. The two parameters play a different role: ε is a perturbation parameter and a is a detuning parameter that is used to fix the dynamics on the torus to a rotation by ω. Hence, varying ε leads to select $a = a(\varepsilon)$ for which there is an invariant torus with frequency ω, and to compute the typical quasi-periodic arcs in $a - \varepsilon$ plane (Peckham and Schilder 2007; Vitolo et al. 2011), which are the continuation curves. We are mostly interested in the transitions of the dynamical properties of the invariant torus along the continuation, and in the mechanisms of breakdown of the torus. We emphasize that our methods let us to perform the continuations up to the tip

of a quasi-periodic arc, at which the torus breaks down. Section 4 presents the models we study further in this paper, provides some guidelines of the implementations, introduces several observables and presents some conjectures on the behavior of the observables at breakdown.

The study of the mechanisms of loss of the hyperbolicity properties of an invariant torus and its breakdown is a subject of strong interest. The most studied scenarios correspond to the deterioration of the rates of contraction and expansion of the linearized dynamics of reducible tori, that go to 1, and concerns the known as *quasi-periodic bifurcation theory* (Broer et al. 1990; Chenciner and Iooss 1979a, b). Besides that, the loss of hyperbolicity can be related with a non-uniform collision of the invariant bundles of the torus, even in cases in which the rates are far from 1, and with loss of reducibility properties. The study of quasi-periodic bifurcations for non-reducible invariant tori is another of the challenging problems stated in Vitolo et al. (2011). Several *bundle merging scenarios* are described in Figueras (2011), Haro and de la Llave (2006b, 2007) for skew-product systems and Calleja and Figueras (2012) for attracting tori in conformally symplectic systems. In this paper, we report the appearance of new bundle merging scenarios in the general dissipative context, providing numerical evidence of universal behavior through several conjectures, which are illustrated in three examples of very different nature. In Sect. 5, we present the breakdown of a saddle invariant torus in a 3D conservative system, due to the collision between the tangent and the stable bundles, which are both of rank 1. In Sect. 6 we describe the several smooth transitions from node to focus and vice versa that an attracting torus of a 3D dissipative system suffers, prior to its destruction by the collision between the tangent and stable bundles, being the stable bundle of rank 2. Finally, in Sect. 7, we report on a subcritical period doubling bifurcation leading to an attracting torus in a 3D dissipative system, and the ulterior non-smooth transitions from reducible to non-reducible and vice versa, geometrically described as non-uniform collisions of the slow and fast stable bundles, which explain the process of *fractalization* that the torus suffers prior its breakdown. The phenomenon of fractalization had been observed in quasi-periodically forced systems (Kaneko 1984; Nishikawa and Kaneko 1996; Sosnovtseva et al. 1996), in the context of strange nonchaotic attractors (Grebogi et al. 1984), and some mechanisms were described in Haro and de la Llave (2006a), Jorba and Tatjer (2008). In retrospective, the non-uniform collisions of the invariant bundles can be understood as the formation of a strange nonchaotic attractor and a strange nonchaotic repeller in the (projective) linearized dynamics (Haro and Puig 2006; Jorba et al. 2007).

2 The Setting

In the following, we consider a smooth family of diffeomorphisms on the annulus $\mathbb{T}^d \times \mathbb{R}^n = (\mathbb{R}/\mathbb{Z})^d \times \mathbb{R}^n$, parameterized by $a \in \mathbb{R}^d$: $F_a : \mathbb{T}^d \times \mathbb{R}^n \to \mathbb{T}^d \times \mathbb{R}^n$. We also assume that each F_a is homotopic to the identity, that is:

$$F_a \begin{pmatrix} x \\ y \end{pmatrix} = \begin{pmatrix} x \\ 0 \end{pmatrix} + F_{a,p} \begin{pmatrix} x \\ y \end{pmatrix},$$

where $F_{a,p}$ is 1-periodic in $x \in \mathbb{T}^d$, $y \in \mathbb{R}^n$.

We also assume that a torus $\mathcal{K}$ is the image of the model torus $\mathbb{T}^d$ by an injective immersion $K : \mathbb{T}^d \to \mathbb{T}^d \times \mathbb{R}^n$ that is homotopic to the zero-section of $\mathbb{T}^d \times \mathbb{R}^n$, and it is of the form

$$K(\theta) = \begin{pmatrix} \theta \\ 0 \end{pmatrix} + K_p(\theta),$$

where $K_p : \mathbb{T}^d \to \mathbb{R}^d \times \mathbb{R}^n$ is 1-periodic in the θ-variables. That is, $\mathcal{K} = K(\mathbb{T}^d)$.

Definition 2.1 We say that the torus $\mathcal{K}$ parameterized by K is F_a-invariant with a quasi-periodic motion given by the frequency $\omega \in \mathbb{R}^d$ if K satisfies the invariance equation

$$F_a(K(\theta)) = K(\theta + \omega). \tag{1}$$

It is clear that the homotopy classes of the dynamical system F_a and of the parameterization K have to match. We could consider other topological properties of F_a and K, and most of below can be repeated with small changes.

Note that (1) is an equation for K and a given the family F_a. Canadell and Haro (2016) provides a theorem of existence of solutions of (1), for smooth families of real-analytic maps. Here and in the following, in order to simplify the explanations of the algorithms, we will not stress regularity properties of the family and of the tori. In any case, a standing hypothesis when using KAM techniques is the Diophantine condition on ω.

Definition 2.2 We say that the frequency vector $\omega \in \mathbb{R}^d$ is (γ, τ)-Diophantine, where $\gamma > 0$ and $\tau \geq d$, if $|\omega \cdot q - p| \geq \gamma |q|_1^{-\tau}$ for any $q \in \mathbb{Z}^d \setminus \{0\}$ and $p \in \mathbb{Z}$.

An important property of an embedded torus is that it is a parallelizable manifold, and it is a framed manifold that possesses a trivialization of a normal bundle in the ambient space. So then, the tangent bundle $\mathrm{T}\mathcal{K}$ is trivial. In particular, the matrix-valued map $L : \mathbb{T}^d \to \mathbb{R}^{(d+n)\times d}$, defined as $L(\theta) = \mathrm{D}K(\theta)$, provides a global frame for the tangent bundle. But, moreover, a normal bundle $\mathrm{N}\mathcal{K}$ can be globally defined by a matrix-valued map $N : \mathbb{T}^d \to \mathbb{R}^{(d+n)\times n}$, so that the column vectors of $L(\theta)$ joined with the column vectors of $N(\theta)$ form a basis of $\mathrm{T}_{K(\theta)}(\mathbb{T}^d \times \mathbb{R}^n) \simeq \mathbb{R}^{d+n}$. In other words, the matrix-valued map $P : \mathbb{T}^d \to \mathbb{R}^{(d+n)\times(d+n)}$, obtained by juxtaposing L and N so that $P(\theta) = \big(L(\theta)\ N(\theta)\big)$, provides an adapted frame around the torus.

Assume now that $\mathcal{K}$, parameterized by K, is F_a-invariant with a fixed frequency ω. By taking derivatives in Eq. (1), we get the invariance equation of the tangent bundle $\mathrm{T}\mathcal{K}$:

$$\mathrm{D}F_a(K(\theta))L(\theta) - L(\theta + \omega) = 0.$$

Then, the linearized dynamics $\mathrm{D}F_a$ around $\mathcal{K}$ in the adapted frame $P(\theta)$ is given by a block triangular matrix valued map $\Lambda : \mathbb{T}^d \to \mathbb{R}^{(d+n)\times(d+n)}$, defined as:

$$\Lambda(\theta) = P(\theta + \omega)^{-1}\mathrm{D}F_a(K(\theta))P(\theta),$$

which is of the form

$$\Lambda(\theta) = \begin{pmatrix} \mathrm{Id} & T(\theta) \\ O & \Lambda_N(\theta) \end{pmatrix},$$

where $\Lambda_N : \mathbb{T}^d \to \mathbb{R}^{n\times n}$, and $T : \mathbb{T}^d \to \mathbb{R}^{d\times n}$ measures the torsion of the normal bundle under the action of $\mathrm{D}F_a \circ K$. It is also desirable to work with a normal bundle $\mathrm{N}\mathcal{K}$ which is also invariant, so that the torsion matrix T is zero. This condition reads as

$$\mathrm{D}F_a(K(\theta))N(\theta) - N(\theta+\omega)\Lambda_N(\theta) = 0. \tag{2}$$

In such a case, the adapted frame P reduces the linearized dynamics to a block diagonal linear skew-product $(\Lambda, R_\omega) : \mathbb{R}^n \times \mathbb{T}^{d+n} \to \mathbb{R}^n \times \mathbb{T}^{d+n}$, so that the linear skew-product $(\Lambda_N, R_\omega) : \mathbb{R}^n \times \mathbb{T}^d \to \mathbb{R}^n \times \mathbb{T}^d$ gives the dynamics on the normal bundle. Here, and in the following, $R_\omega : \mathbb{T}^d \to \mathbb{T}^d$ denotes the rotation by ω: $R_\omega(\theta) = \theta + \omega$. From now on, we will consider the normal bundle invariant.

We are going now to give some definitions of normal hyperbolicity adapted to the setting of this paper. For more general and detailed definitions, see Canadell and Haro (2016). We will assume that the stable and unstable bundles are trivial. Since there are cases in which non-trivial (non-orientable) bundles are easily trivialized by using a double covering trick, we will consider the frame P defined from $\tilde{\mathbb{T}}^d = (\mathbb{R}/2\mathbb{Z})^d$ instead of $\mathbb{T}^d$.

Definition 2.3 We say that the invariant torus is *hyperbolically block-diagonalizable* (by the adapted frame P) if $n_s + n_u = n$ and $\Lambda_N(\theta) = \mathrm{blockdiag}(\Lambda_S(\theta), \Lambda_U(\theta))$, where the linear skew-products $(\Lambda_S, R_\omega) : \mathbb{R}^{n_s} \times \tilde{\mathbb{T}}^d \to \mathbb{R}^{n_s} \times \tilde{\mathbb{T}}^d$, $(\Lambda_U, R_\omega) : \mathbb{R}^{n_u} \times \tilde{\mathbb{T}}^d \to \mathbb{R}^{n_u} \times \tilde{\mathbb{T}}^d$ are uniformly contracting and expanding, respectively.

Sometimes, it is possible to choose a frame in such a way that the linearization becomes a constant matrix.

Definition 2.4 We say that the invariant torus is *reducible* to a constant matrix (by the adapted frame P) if Λ_N is a constant $n \times n$ matrix. We will refer to the eigenvalues of Λ_N as to the eigenvalues or Floquet multipliers of the torus.

There are cases in which, moreover, there are n different rates of growth.

Definition 2.5 We say that the invariant torus is *completely reducible* (by the adapted frame P) if the normal dynamics is reduced to a diagonal real constant matrix $\Lambda_N = \mathrm{diag}(\lambda_{d+1}, \ldots, \lambda_{d+n})$, with different entries, which are the eigenvalues or Floquet multipliers of the torus.

Reducibility properties are very important in dynamics, since they provide full information about the linearization around an invariant torus, see Eliasson (2001), Jorba and Simó (1992, 1996). These reducibility properties, which are usually present in KAM theory, are, however, often violated. We will present several examples in the context of this paper in which reducibility properties do not hold.

In the following, we present three different algorithms for the computation of quasi-periodic invariant tori in the three cases defined above. Two of them are adapted to reducible tori, and the other works in non-reducible cases.

3 Three Newton-Like Algorithms for Computing Quasi-Periodic Tori

In the setting defined in the previous section, our goal is to compute a parameterization K of a quasi-periodic normally hyperbolic invariant torus (QP-NHIT for short) under F_a by adjusting the detuning parameter a, as well as their invariant normal bundles. In the following, we explain how to perform one step of a Newton-like method to solve the invariance equations (1) and (2). The specific form of Λ_N determines three different algorithms.

We start with a parameterization K of an approximate QP-NHIT and its corresponding parameter a, an approximate invariant normal bundle N and its linearized dynamics Λ_N. That is, the error functions $E : \mathbb{T}^d \to \mathbb{R}^{d+n}$ and $E_{\text{red}} : \mathbb{T}^d \to \mathbb{R}^{(d+n)\times(d+n)}$ defined as

$$E(\theta) = F_a(K(\theta)) - K(\theta + \omega), \tag{3}$$

$$E_{\text{red}}(\theta) = P(\theta + \omega)^{-1} \mathrm{D}F_a(K(\theta))P(\theta) - \Lambda(\theta), \tag{4}$$

which give the error in the invariance equation of the torus and the error in the linearized dynamics, respectively, are assumed to be "small" (using appropriate norms). Then, the aim of one step of the Newton-like method is to compute their corresponding corrections $\Delta K, \Delta a, \Delta N, \Delta_N$ and to obtain new better approximations $\bar{K} = K + \Delta K, \bar{a} = a + \Delta a, \bar{N} = N + \Delta N, \bar{\Lambda}_N = \Lambda_N + \Delta_N$. Hence, under appropriate non-degeneracy properties and the smallness of the errors, the error estimates of the new approximations are quadratically small with respect to the initial errors. The procedure is repeated until we achieve the desired error tolerance.

Since we are working with periodic functions to represent the objects and the internal dynamics is a rotation R_ω, it is natural to represent them in Fourier series. Then, if f is a periodic function, we denote by

$$f(\theta) = \sum_{k \in \mathbb{Z}^d} f_k e^{2\pi \mathbf{i} k\theta}$$

its Fourier series. Also, the average of f is defined as $\langle f \rangle = f_0$.

3.1 Substep 1: Correction of the Torus K and Its Parameter a

We consider the correction of the torus expressed in terms of the adapted frame, as $\Delta K(\theta) = P(\theta)\xi(\theta)$ where $\xi : \mathbb{T}^d \to \mathbb{R}^{d+n}$ is a periodic function. Note that the correction preserves the homotopy class of the torus. Then, by substituting the new approximations $\bar{K}$ and $\bar{a}$ in (1) and using first-order Taylor expansions, we obtain the following expression

$$\begin{aligned} 0 &= F_a(K(\theta) + P(\theta)\xi(\theta)) - K(\theta+\omega) - P(\theta+\omega)\xi(\theta+\omega) \\ &= F_a(K(\theta)) + \mathrm{D}F_a(K(\theta))P(\theta)\xi(\theta) + \frac{\partial F_a}{\partial a}(K(\theta))\Delta a \\ &\quad - K(\theta+\omega) - P(\theta+\omega)\xi(\theta+\omega) + \mathcal{O}_2 \\ &= E(\theta) + \frac{\partial F_a}{\partial a}(K(\theta))\Delta a + P(\theta+\omega)\Lambda(\theta)\xi(\theta) - P(\theta+\omega)\xi(\theta+\omega) + \mathcal{O}_2, \end{aligned} \tag{5}$$

where we apply definitions (3) and (4) above, and $\mathcal{O}_2$ collect the quadratically small terms. Then, multiplying the previous expression (5) by $P(\theta+\omega)^{-1}$ and neglecting the quadratically small terms, we obtain the following cohomological equation

$$\eta(\theta) = \Lambda(\theta)\xi(\theta) - \xi(\theta+\omega) + B(\theta)\Delta a, \tag{6}$$

where $\eta(\theta) = -P(\theta+\omega)^{-1}E(\theta)$ represents the error of the approximate solution (K, a) in the adapted frame and $B(\theta)$ is given by

$$B(\theta) = P(\theta+\omega)^{-1}\frac{\partial F_a}{\partial a}(K(\theta)).$$

Since Λ is a block diagonal matrix with blocks the identity matrix and Λ_N, we split Eq. (6) into tangent and normal components, so that the substep reduces to solving the following block diagonal system:

$$\eta^L(\theta) - B^L(\theta)\Delta a = \xi^L(\theta) - \xi^L(\theta+\omega), \tag{7}$$
$$\eta^N(\theta) - B^N(\theta)\Delta a = \Lambda_N(\theta)\xi^N(\theta) - \xi^N(\theta+\omega). \tag{8}$$

We will use the indices ^{L} and ^{N} for the tangent and normal components.

3.1.1 Tangent Cohomological Equation

We have to solve Eq. (7). To do so, we first choose the correction Δa as

$$\Delta a = -\langle B^L\rangle^{-1}\langle \eta^L\rangle, \tag{9}$$

provided that $\langle B^L(\theta)\rangle$ is an invertible matrix, so that the left-hand size of (7) has zero average.

Remark 3.1 In this setting, the correction of the detuning parameter a has a clear geometrical and dynamical explanation: it is made along the tangent bundle of the torus in order to fix the internal dynamics.

In particular, Eq. (7) splits into d equations corresponding to the d tangent directions:

$$\xi^i(\theta) - \xi^i(\theta+\omega) = \tilde{\eta}^i(\theta), \tag{10}$$

where $\tilde{\eta}(\theta) := \eta(\theta) - B(\theta)\Delta a$, for $i = 1, \ldots, d$, and with Δa known. Hence, the solution of each equation (10), for $i = 1, \ldots, d$, is obtained by solving them order by order in terms of their Fourier modes:

$$\xi_k^i = \frac{\eta_k^i - (B_k^L \Delta a)^i}{1 - e^{2\pi i k\omega}}, \ k \neq 0.$$

Notice that denominators do not vanish since rotation ω is assumed to be Diophantine. Notice also that the first mode ξ_0^i is free.

Remark 3.2 In Canadell and Haro (2016), we gave an explicit formula for this term ξ_0^i to obtain a zero average of the periodic first component of the torus. In this paper, we choose $\xi_0^i = 0$ for all i to simplify. The normalization $\langle K_p^x \rangle = 0$ can be done at the end of the procedure.

3.1.2 Normal Cohomological Equation

Once we have obtained the tangent correction of the torus and the correction of the adjusting parameter a, we compute the normal correction by solving Eq. (8). We redefine now Eq. (8) as:

$$\tilde{\eta}^N(\theta) = \Lambda_N(\theta)\xi^N(\theta) - \xi^N(\theta + \omega), \tag{11}$$

where $\tilde{\eta}^N(\theta) := \eta^N(\theta) - B^N(\theta)\Delta a$ is known, since Δa is given by (9). Then, the specific form of Λ_N gives us three different ways of solving Eq. (11). We will detail these three different cases later in Sect. 3.3.

At the end of this first step of the algorithm, we obtain new approximations $\bar{K}$ and $\bar{a}$ for which the new error $\bar{E}(\theta) = F_{\bar{a}}(\bar{K}(\theta)) - \bar{K}(\theta + \omega)$ is quadratically small with respect to $E(\theta)$. We then redefine $K = \bar{K}$, $a = \bar{a}$ and recompute P.

3.2 Substep 2: Correction of the Normal Bundles

We recompute the error $E_{\text{red}}(\theta)$ in (4) for the new values K and a. We look for the correction of N of the form $\Delta N(\theta) = P(\theta)Q^N(\theta)$, where $Q^N : \mathbb{T}^d \to \mathbb{R}^{(d+n)\times n}$ is a periodic matrix map, and the correction Δ_N, to obtain new approximations $\bar{N}$ and $\bar{\Lambda}_N$. By substituting $\bar{N}$ and $\bar{\Lambda}_N$ in Eq. (2), we obtain

$$\begin{aligned}
0 &= DF(K(\theta))\bar{N}(\theta) - \bar{N}(\theta + \omega)\bar{\Lambda}_N(\theta) \\
&= DF(K(\theta))\left(N(\theta) + P(\theta)Q^N(\theta)\right) \\
&\quad - \left(N(\theta + \omega) + P(\theta + \omega)Q^N(\theta + \omega)\right)\left(\Lambda_N(\theta) + \Delta_N(\theta)\right) \\
&= P(\theta + \omega)E_{\text{red}}^N(\theta) + \left(P(\theta + \omega)\Lambda(\theta) + P(\theta + \omega)E_{\text{red}}(\theta)\right)Q^N(\theta) \\
&\quad - P(\theta + \omega)Q^N(\theta + \omega)\Lambda_N(\theta) - N(\theta + \omega)\Delta_N(\theta) \\
&\quad - P(\theta + \omega)Q^N(f(\theta))\Delta_N(\theta).
\end{aligned}$$

Hence, by multiplying the previous equation by $P(\theta+\omega)^{-1}$ and neglecting quadratically small terms, we obtain the following cohomological equation:

$$-E^N_{\mathrm{red}}(\theta) = \Lambda(\theta)Q^N(\theta) - Q^N(\theta+\omega)\Lambda_N(\theta) - \begin{pmatrix} O \\ \Delta_N(\theta) \end{pmatrix}.$$

Finally, by writing the correction matrix Q^N as

$$Q^N(\theta) = \begin{pmatrix} Q^{LN}(\theta) \\ Q^{NN}(\theta) \end{pmatrix},$$

where Q^{LN} is a $d \times n$ matrix and Q^{NN} is a $n \times n$ matrix, the equation above splits into the following two equations:

$$-E^{LN}_{\mathrm{red}}(\theta) = Q^{LN}(\theta) - Q^{LN}(\theta+\omega)\Lambda_N(\theta), \tag{12}$$
$$-E^{NN}_{\mathrm{red}}(\theta) = \Lambda_N(\theta)Q^{NN}(\theta) - Q^{NN}(\theta+\omega)\Lambda_N(\theta) - \Delta_N(\theta). \tag{13}$$

The way to solve these two equations depends on the form of Λ_N. We will detail the different options in the following subsection.

Remark 3.3 We can solve numerically Eqs. (11), (12) and (13) by their straightforward discretization in Fourier modes, to obtain large linear systems of equations whose unknowns are the Fourier coefficients. The methods we present here rely in dynamical properties of the torus that avoid solving large linear systems.

Summarizing, after the second substep, we obtain new approximations $\bar{N}$ and $\bar{\Lambda}_N$, and so a new adapted frame $\bar{P}(\theta) = \left(\bar{L}(\theta)\ \bar{N}(\theta)\right)$, that improves the error $E_{\mathrm{red}}(\theta)$. We have to repeat substeps 1 and 2 until we reach the desired error tolerance.

3.3 Specification of the Algorithms

Whereas the solution of Eq. (7) does not depend on Λ_N, the form we choose for Λ_N provides different ways to solve Eqs. (11), (12) and (13).

3.3.1 An Algorithm Based on Hyperbolic Block-Diagonalizability

If we assume that the invariant torus is hyperbolically block-diagonalizable, then the matrix-valued map $\Lambda_N(\theta)$ is a block diagonal matrix with contracting and expanding submatrices, see Definition 2.3. Consequently, Eq. (11) splits into stable and unstable components:

$$\tilde{\eta}^S(\theta) = \Lambda_S(\theta)\xi^S(\theta) - \xi^S(\theta+\omega), \tag{14}$$
$$\tilde{\eta}^U(\theta) = \Lambda_U(\theta)\xi^U(\theta) - \xi^U(\theta+\omega), \tag{15}$$

and Eq. (12) splits into the following two equations:

$$-E^{LS}_{\mathrm{red}}(\theta) = Q^{LS}(\theta) - Q^{LS}(\theta+\omega)\Lambda_S(\theta), \tag{16}$$
$$-E^{LU}_{\mathrm{red}}(\theta) = Q^{LU}(\theta) - Q^{LU}(\theta+\omega)\Lambda_U(\theta). \tag{17}$$

Also, in this setting, the corrections of the (approximate) stable and unstable bundles are performed in the complementary directions. That is, the correction matrix Q^{NN} is chosen as follows

$$Q^{NN}(\theta) = \begin{pmatrix} O & Q^{SU}(\theta) \\ Q^{US}(\theta) & O \end{pmatrix},$$

so that the "missing" blocks Q^{SS} and Q^{UU} are taken to be zero. Hence, Eq. (13) splits into the four different equations below:

$$-E^{US}_{\mathrm{red}}(\theta) = \Lambda_U(\theta)Q^{US}(\theta) - Q^{US}(\theta+\omega)\Lambda_S(\theta), \tag{18}$$
$$-E^{SU}_{\mathrm{red}}(\theta) = \Lambda_S(\theta)Q^{SU}(\theta) - Q^{SU}(\theta+\omega)\Lambda_U(\theta), \tag{19}$$
$$-E^{SS}_{\mathrm{red}}(\theta) = -\Delta_S(\theta), \tag{20}$$
$$-E^{UU}_{\mathrm{red}}(\theta) = -\Delta_U(\theta), \tag{21}$$

from which we obtain directly the correction of the linearized normal dynamics in Eqs. (20) and (21).

Notice that Eqs. (14), (15), (16), (17), (18), (19) are solvable under hyperbolicity conditions by simple iteration using the contracting principle, which will converge to the solutions ξ^S, ξ^U, Q^{LS}, Q^{LU}, Q^{SU} and Q^{US}, respectively.

Remark 3.4 Fast iterative methods for solving cohomology equations (14), (15), (16), (17), (18), (19) have been designed in Huguet et al. (2013) (see also Canadell 2014), reducing m iterations of simple iteration method to $\log_2 m$.

3.3.2 An Algorithm Based on Reducibility

We consider here the reducible case, that is, we assume Λ_N is a constant matrix, see Definition 2.4. Then, we rewrite Eqs. (11) and (12) in terms of the Fourier coefficients as follows:

$$\tilde{\eta}^N_k = \Lambda_N \xi^N_k - \xi^N_k e^{2\pi \mathbf{i} k\omega}, \tag{22}$$
$$-E^{LN}_{\mathrm{red}\,k} = Q^{LN}_k - Q^{LN}_k e^{2\pi \mathbf{i} k\omega}\Lambda_N. \tag{23}$$

By normal hyperbolicity, the term $(\Lambda_N - e^{2\pi \mathbf{i} k\omega}\mathrm{Id})$ is invertible for all $k \in \mathbb{Z}^d$, and we get the solution of Eq. (22) by isolating the term ξ^N_k:

$$\xi^N_k = (\Lambda_N - e^{2\pi \mathbf{i} k\omega}\mathrm{Id})^{-1}\tilde{\eta}^N_k,$$

for each k. Moreover, we solve Eq. (23) by isolating the unknown Q_k^{LN}, and its corresponding solution is

$$Q_k^{LN} = -E_{\mathrm{red}\,k}^{LN}\left(\mathrm{Id} - e^{2\pi \mathbf{i} k\omega}\Lambda_N\right)^{-1},$$

for all $k \in \mathbb{Z}^d$.

Remark 3.5 In general, the condition for the matrix $(\Lambda_N - e^{2\pi \mathbf{i} k\omega})$ to be invertible for all $k \in \mathbb{Z}^d$, that is

$$\lambda - e^{2\pi \mathbf{i} k\omega} \neq 0,$$

for each $\lambda \in \mathrm{Spec}(\Lambda_N)$, is referred to as a *first Melnikov condition*. One can also consider directions in the normal bundle that are *normally elliptic*, that correspond to complex eigenvalues of modulus 1. We emphasize that, in KAM theory, Melnikov condition is Diophantine-like.

Since Λ_N is a constant matrix, then so is its correction Δ_N. Hence, we rewrite Eq. (13) in terms of Fourier coefficients as the following system:

$$-E_{\mathrm{red}\,0}^{NN} = \Lambda_N Q_0^{NN} - Q_0^{NN}\Lambda_N - \Delta_N, \quad k = 0, \tag{24}$$

$$-E_{\mathrm{red}\,k}^{NN} = \Lambda_N Q_k^{NN} - Q_k^{NN} e^{2\pi \mathbf{i} k\omega}\Lambda_N, \quad k \neq 0. \tag{25}$$

By choosing $Q_0^{NN} = 0$ in Eq. (24), which corresponds to the constant Fourier term, we obtain the correction of the dynamics on the normal bundles, which is of the form

$$\Delta_N = E_{\mathrm{red}\,0}^{NN}.$$

Then, to obtain the other $k \neq 0$ Fourier terms of the solution Q^{NN}, we solve Eqs. (25) as n^2-dimensional linear systems.

Remark 3.6 The hypothesis for solvability of Eq. (25) for all $k \in \mathbb{Z}^d \setminus \{0\}$ is a *second Melnikov condition*

$$\lambda_i - e^{2\pi \mathbf{i} k\omega}\lambda_j \neq 0,$$

where $\lambda_i, \lambda_j \in \mathrm{Spec}(\Lambda_N)$ (again, in KAM theory the appropriate condition is stronger). In particular, real and complex Floquet multipliers, that is, the eigenvalues on Λ_N, can appear in the reducible case.

Remark 3.7 Notice that in this case, instead of solving Eqs. (11), (12) and (13) by using simple iteration as in the algorithm based on hyperbolic block-diagonalizability, we solve them term by term in Fourier modes. This update leads to a faster algorithm, as long as the torus is reducible.

3.3.3 An Algorithm Based on Complete Reducibility

We consider now the completely reducible case, see Definition 2.5. Hence, we assume $\Lambda_N = \mathrm{diag}(\lambda_{d+1}, \ldots, \lambda_{d+n})$ and its correction is of the form $\Delta_N = \mathrm{diag}(\delta_{d+1}, \ldots, \delta_{d+n})$. Then, Eq. (11) splits into n equations corresponding to their n normal components, which are diagonalized in the Fourier space:

$$\tilde{\eta}_k^i = \lambda_i \xi_k^i - e^{2\pi \mathbf{i} k\omega} \xi_k^i,$$

for $i = d+1, \ldots, d+n, k \in \mathbb{Z}^d$. Then, as long as a first Melnikov condition is satisfied, see Remark 3.5, the Fourier coefficients of the solutions are

$$\xi_k^i = \frac{\tilde{\eta}_k^i}{\lambda_i - e^{2\pi \mathbf{i} k\omega}}, \tag{26}$$

for $i = d+1, \ldots, d+n, k \in \mathbb{Z}^d$. In particular, under the condition of normal hyperbolicity, $|\lambda_i| \neq 1$ for all i, and there are no resonances in (26).

Equations (12) and (13) are also diagonal in the Fourier space. In this case, we use the following notation for the correction of the bundles

$$Q^N(\theta) = (Q^{i,j}(\theta)),$$

where $i = 1, \ldots, n+d$, $j = d+1, \ldots, d+n$. Then, Eqs. (12) and (13) split into $(d+n) \times n$ equations, which can be classified in the following three different equation types:

$$\begin{aligned}
i \leq d,\ i \neq j:\ & -E_{\mathrm{red}}^{i,j}(\theta) = Q^{i,j}(\theta) - Q^{i,j}(\theta+\omega)\lambda_j, \\
i > d,\ i \neq j:\ & -E_{\mathrm{red}}^{i,j}(\theta) = \lambda_i Q^{i,j}(\theta) - Q^{i,j}(\theta+\omega)\lambda_j, \\
i > d,\ i = j:\ & -E_{\mathrm{red}}^{i,i}(\theta) = \lambda_i Q^{i,i}(\theta) - Q^{i,i}(\theta+\omega)\lambda_i - \delta^i,
\end{aligned}$$

for $j = d+1, \ldots, d+n$. We solve each of these three equations in terms of Fourier modes, obtaining:

$$i \leq d,\ i \neq j:\ Q_k^{i,j} = \frac{\left(E_{\mathrm{red}}^{i,j}\right)_k}{\lambda_j e^{2\pi \mathbf{i} k\omega} - 1}, \quad \forall k \in \mathbb{Z}^d.$$

$$i > d,\ i \neq j:\ Q_k^{i,j} = \frac{\left(E_{\mathrm{red}}^{i,j}\right)_k}{\lambda_j e^{2\pi \mathbf{i} k\omega} - \lambda_i}, \quad \forall k \in \mathbb{Z}^d.$$

$$i > d,\ i = j:\ Q_k^{i,i} = \begin{cases} \dfrac{\left(E_{\mathrm{red}}^{i,i}\right)_k}{\lambda_i (e^{2\pi \mathbf{i} k\omega} - 1)}, & k \neq 0, \\ 0, & k = 0, \end{cases} \quad \delta_i = \left(E_{\mathrm{red}}^{i,i}\right)_0.$$

Again, these equations are solvable as long as a second Melnikov condition is satisfied, see Remark 3.6. This is the case, for instance, under normal hyperbolicity properties and with the complete reducibility assumption $|\lambda_i| \neq |\lambda_j| \neq 1$ for $i \neq j$.

Remark 3.8 In the implementation of reducibility methods, one can consider complex entries in the matrices Λ_N and Δ_N, just appealing to the complexification trick. One has to be aware of resonances. See Haro and de la Llave (2007) for some implementations of methods to cross resonances.

4 On the Implementation of the Algorithms and Conjectures of Their Breakdown

In this section, we are going to provide some details of the implementations of the algorithms explained in the previous section. We will also present several observables to monitor hyperbolicity and reducibility properties of the tori. These will be used in further sections to describe the dynamical properties along the continuations of tori.

4.1 The Models

We have implemented the algorithms of this paper for the continuation of invariant tori of dimension 1 with a prescribed frequency, in two 2-parameter families of diffeomorphisms in $\mathbb{T} \times \mathbb{R}^2$. Notice, however, that in the following systems the torus is defined as $\mathbb{R}/2\pi\mathbb{Z}$ (instead of $\mathbb{R}/\mathbb{Z}$), and slight modifications of the algorithms given in previous section are in order.

The first model we consider is the 3D-*Fattened Arnold Family* (3D-FAF) (Broer et al. 1997) given by $F_{a,\varepsilon} : \mathbb{R}/2\pi\mathbb{Z} \times \mathbb{R}^2 \to \mathbb{R}/2\pi\mathbb{Z} \times \mathbb{R}^2$ defined as:

$$F_{a,\varepsilon}\begin{pmatrix} x \\ y \\ z \end{pmatrix} = \begin{pmatrix} x + a + \varepsilon(\sin(x) + y + z/2) \\ b(\sin(x) + y) \\ c(\sin(x) + y + z) \end{pmatrix} \tag{29}$$

where b, c are fixed parameters, $a \in \mathbb{R}$ is the adjusting parameter and $\varepsilon \in \mathbb{R}$ is the continuation parameter. Notice that this family has a constant determinant of the Jacobian $\det(\mathrm{D}F_{a,\varepsilon}) = bc$, so we can choose different parameters b and c in order to explore different examples of normally hyperbolic invariant tori in conservative and dissipative cases. In particular, in Sect. 5 we discuss the computation of quasi-periodic saddle tori for a conservative case ($b = 0.25$, $c = 4$) and in Sect. 6 we study the many node-focus transitions on the linearized dynamics of attracting tori for a dissipative case ($b = 0.5$, $c = 0.4$).

The second model we consider is the 3D-*Fattened Hénon Family* (3D-FHF), given by $F_{a,\varepsilon} : \mathbb{R}/2\pi\mathbb{Z} \times \mathbb{R}^2 \to \mathbb{R}/2\pi\mathbb{Z} \times \mathbb{R}^2$ defined as:

$$F_{a,\varepsilon}\begin{pmatrix} x \\ y \\ z \end{pmatrix} = \begin{pmatrix} x + a + d\varepsilon(\cos(x) + z) \\ 1 + z - by^2 + \varepsilon\cos(x) \\ cy \end{pmatrix} \tag{30}$$

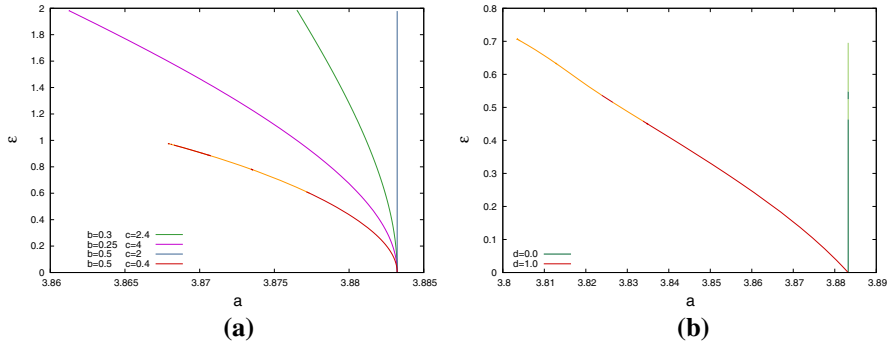

Fig. 1 Quasi-periodic arcs in the (a, ε)-plane for several families. **a** 3D-FAF: the *purple arc* corresponds to Sect. 5 (b = 0.25, c = 4), where tori are saddle type, and *orange–red arc* corresponds to Sect. 6 (b = 0.5, c = 0.4), where tori are attracting, either node type (*red*) or focus type (*orange*). **b** 3D-FHF ($b = 0.68$, $c = 0.1$): the *red–orange arc* corresponds to the skew-product case $d = 0$ and the *green–light green arc* corresponds to $d = 1$, detailed in Sect. 7, where tori are either reducible (*red–green*) or non-reducible (*orange–light green*) (Color figure online)

where b, c, d are fixed parameters, $a \in \mathbb{R}$ is the adjusting parameter and $\varepsilon \in \mathbb{R}$ is the continuation parameter. This family is an extension of the *rotating Hénon Family*, studied in Haro and de la Llave (2007), that corresponds to $d = 0$. In this paper, see Sect. 7, we take $d = 1$ and continue a saddle torus that bifurcates into an attracting node torus, that suffers many reducible/non-reducible transitions on the linearized dynamics that precede the breakdown of the torus.

For the previous models, and once we have fixed the internal parameters (b, c, d), we continue with respect to parameter ε a normally hyperbolic invariant torus with frequency the golden mean $\omega = (\sqrt{5} - 1)\pi$, parameterized by $K = K_\varepsilon$, and the corresponding adjusting parameter $a = a(\varepsilon)$. These computations produce the so-called *quasi-periodic arcs* (for the golden mean frequency) in the parameter plane (a, ε). We have implemented the algorithms presented in this paper by applying Fourier methods. In particular, we compute invariant tori and their invariant normal bundles and their internal dynamics. Figure 1 summarizes the computations, showing different quasi-periodic arcs. A more detailed explanation will be given in the following sections with the aid of several observables (Lyapunov multipliers, angles between bundles, C^r and Sobolev norms) that we will introduce later in this section. We are interested not only in the dynamical phenomena that appear during the continuation, but also to the mechanisms of breakdown that happen at the tip of the quasi-periodic arcs.

4.2 Fourier Approximations

In the implementation of the algorithms for the examples introduced in the previous section, we use (truncated) Fourier series approximations with a given number N_{F} of harmonics to approximate 2π-periodic functions (notice that the angle variable in the examples is defined modulus 2π). This is very appropriate, since the algorithms include the solution of cohomological equations and compositions with rotations (such

as $K \circ R_\omega$). Given a periodic function $g : [0, 2\pi] \to \mathbb{R}$, a (truncated) Fourier series approximation is a trigonometric polynomial of the form

$$\hat{g}(\theta) = \hat{c}_0 + \sum_{k=1}^{N_F} \left(\hat{c}_k \cos(k\theta) + \hat{s}_k \sin(k\theta) \right), \tag{31}$$

which is an approximation of the Fourier series

$$g(\theta) = c_0 + \sum_{k=1}^{\infty} \left(c_k \cos(k\theta) + s_k \sin(k\theta) \right), \tag{32}$$

whose amplitudes $\sqrt{c_k^2 + s_k^2}$ decrease rapidly to zero since we assume g to be a smooth (or even real-analytic) periodic function. In order to control error estimates in the invariance equations, we use norms in Fourier space, such as the $W^{0,1}$ norm of the trigonometric polynomial approximation,

$$||\hat{g}||_{W^{0,1}} = |\hat{c}_0| + \sum_{k=1}^{N_F} \sqrt{\hat{c}_k^2 + \hat{s}_k^2}.$$

We can extend the definition component-wise to vectors and matrices of (approximations of) periodic functions.

Other parts of the algorithms consist in composing periodic functions with the equations of the model (i.e. $F(K(\theta))$, and algebraic operations. In this respect, it is very useful to compute grid approximations, then do these operations in grid space, and go back to Fourier space to obtain Fourier approximations of the operations. A grid approximation of the function g is just an ordered set

$$\{g_i\} = \{g_i = g(\theta_i)\}_{i=0}^{2N_F} \tag{33}$$

of evaluations of the function on the mesh $\left\{\theta_i = \frac{2\pi i}{2N_F+1} \mid i = 0, \ldots, 2N_F\right\}$. It is well known that there are very efficient ways of going from the Fourier representation (31) to the grid representation (33), and vice versa, of cost $O(N_F \log N_F)$, by means of backward and forward fast Fourier transforms (FFT). One can also obtain error bounds in the approximations of the Fourier coefficients in (32) by discrete Fourier transform (31) (Epstein 2005; Figueras et al. 2016).

With the aid of basic routines to manipulate trigonometric polynomials and FFT, we can implement the different algorithms presented in this paper. In reducible cases, the algorithms simplify to equations that are diagonal in the Fourier space, so it becomes faster to solve. In particular, we need $O(N_F)$ storage space and $O(N_F \log N_F)$ operations in order to perform a Newton step combined with FFT routines.

In the continuation process with respect to parameter ε, we control the step size $\Delta\varepsilon$ and adapt the number of Fourier modes N_F in order to get error tolerances and tails of Fourier expansions smaller than 10^{-10} when solving the invariance equations.

Table 1 Computation time of one Newton step for the different algorithms of this paper by using a usual laptop

N_F	Completely red.	Red.	Hyp. block-diag.
128	0.0506	0.0860	0.1700
256	0.1294	0.2250	0.4475
512	0.2473	0.3133	0.5440
1024	0.4302	0.7150	1.2750
2048	0.9333	0.7350	1.3875
4096	1.4187	1.3700	2.5525
8192	2.8907	2.0400	3.8125
16,384	5.2750	5.9625	10.2050
32,768	11.6475	11.9700	24.4850
65,536	21.0425	21.0575	43.9350
131,072	51.3425	50.7920	104.690
262,144	79.2025	75.7500	151.110
524,288	140.776	170.220	274.075
1,048,576	346.405	406.400	664.240

The continuation stops when the torus reaches $2^{20} = 1{,}048{,}576$ Fourier modes or the step size is smaller than 10^{-7}. See Table 1 for the computation time (in seconds) of a Newton step for all the three different algorithms explained in this paper.

We should remark that we can perform continuations till breakdown because we use efficient methods which allow us to do reliable computations using a large number of Fourier modes, which are unapproachable by standard large matrix methods. Moreover, the breakdown of the computation happens when the dynamical properties of the torus deteriorate, which takes place just before the breakdown of the object is engendered.

4.3 Functional Observables and Their Blow Up at Breakdown

In order to monitor the quality of the regularity of the torus in a continuation process, we measure its Sobolev norms (Calleja and de la Llave 2009; de la Llave and Luque 2011) and C^r norms. These are suitable to detect the breakdown of the torus when varying the perturbation parameter, since in such a situation these norms experiment a blow up at a critical value. This is in contrast with smooth bifurcations such as saddle-node or period doubling, in which the norms remain bounded.

For a real-analytic periodic function $g : [0, 2\pi] \to \mathbb{C}$, we define the fractional derivative $g^{(r)} : [0, 2\pi] \to \mathbb{C}$, for any $r > 0$, through the Fourier expansions:

$$g^{(r)}(\theta) = \sum_{k=1}^{\infty} k^r \left(\left(\cos\left(\tfrac{\pi}{2} r\right) c_k + \sin\left(\tfrac{\pi}{2} r\right) s_k \right) \cos(k\theta) + \left(\cos\left(\tfrac{\pi}{2} r\right) s_k - \sin\left(\tfrac{\pi}{2} r\right) c_k \right) \sin(k\theta) \right).$$

Then, the C^r-seminorm of g is the sup-norm of $g^{(r)}$,

$$||g||_{C^r} = ||g^{(r)}||_\infty = \max_{\theta\in[0,2\pi]} \left|g^{(r)}(\theta)\right|, \tag{34}$$

and the $W^{r,p}$-seminorm of g is the ℓ_p-norm of $g^{(r)}$:

$$||g||_{W^{r,p}} = \left(\sum_{k=1}^{\infty} \left(k^r \sqrt{s_k^2 + c_k^2}\right)^p\right)^{\frac{1}{p}}. \tag{35}$$

Notice that, from the Hölder inequality with $\frac{1}{q} + \frac{1}{p} = 1$, we get the bounds

$$||g||_{C^r} \leq ||g||_{W^{r,1}} \leq \left(\sum_{k>0} 2k^{(r-s)q}\right)^{\frac{1}{q}} ||g||_{W^{s,p}},$$

as long as $r < s - \frac{1}{q}$. That is, the inclusion $W^{s,p} \subset W^{r,1}$ is closed. We will mainly consider Sobolev seminorms $H^s = W^{s,2}$.

The numerical approximations of these seminorms are obtained from the grid and trigonometric polynomial approximations of g. Notice that the C^r-seminorm of g in (34) can be estimated from the grid representation of the r-derivative of the trigonometric polynomial approximation $\hat{g}$, while the $W^{r,p}$-seminorm in (35) can be estimated directly from $\hat{g}$.

In the applications of the following three sections, we will consider the blow up of the C^r and H^r seminorms in order to detect and to study the destruction of invariant tori (in connection with renormalization group theory). The conjecture that formulates this idea is given below.

Conjecture 4.1 *Let $F_{a,\varepsilon} : \mathbb{T}\times\mathbb{R}^n \to \mathbb{T}\times\mathbb{R}^n$ be a family of real-analytic maps, where a is the adjusting parameter and ε is the continuation parameter. Let $(K_\varepsilon, a_\varepsilon)$ be a family of quasi-periodic normally hyperbolic invariant tori parameterized by $K_\varepsilon : \mathbb{T} \to \mathbb{T}\times\mathbb{R}^n$ and their adjusting parameters, where $\varepsilon \in [0, \varepsilon_c[$. Then, when the torus breaks down at a critical value ε_c, the Sobolev and C^r critical regularities of the torus are r_c and $\hat{r}_c$, respectively, and:*

- *for $r > r_c$ the H^r seminorm blows up as*

$$||K_\varepsilon^x - \mathrm{id}||_{H^r} \sim \frac{A_r}{(\varepsilon_c - \varepsilon)^{B_r}}, \tag{36}$$

  when $\varepsilon \to \varepsilon_c$, with a critical exponent $B_r = a + br$, with $r_c = -\frac{a}{b}$;
- *for $r > \hat{r}_c$ the C^r seminorm blows up as*

$$||K_\varepsilon^x - \mathrm{id}||_{C^r} \sim \frac{\hat{A}_r}{(\varepsilon_c - \varepsilon)^{\hat{B}_r}}, \tag{37}$$

when $\varepsilon \to \varepsilon_c$, *with a critical exponent* $\hat{B}_r = \hat{a} + \hat{b}r$, *with* $\hat{r}_c = -\frac{\hat{a}}{\hat{b}}$.

Remark 4.2 These constants $a, b, \hat{a}, \hat{b}$ of the critical exponents B_r and $\hat{B}_r$ characterize a universal class of breakdown, as well as the critical regularities r_c and $\hat{r}_c$. Notice that, from Sobolev inequalities, $\hat{r}_c \geq r_c - \frac{1}{2}$.

Remark 4.3 In the implementations, the conjectured behavior in the blow up of Sobolev and C^r seminorms when approaching the breakdown of the torus are very useful to extrapolate the critical parameter ε_c, as well as to estimate the critical regularities r_c and $\hat{r}_c$ of the torus at breakdown.

4.4 Dynamical Observables and Their Behavior at Transitions and Breakdowns

The linearized dynamics around a quasi-periodic $F_{a,\varepsilon}$-invariant torus $\mathcal{K}_\varepsilon$, parameterized by K_ε and whose internal dynamics is a rotation R_ω, is provided by the linear skew-product $(\mathrm{D}F_{a,\varepsilon} \circ K_\varepsilon, R_\omega)$. Important information about stability is given by its *Lyapunov multipliers*. By using the adapted frame P, one obtains a conjugate linear skew-product (Λ, R_ω) which is in block diagonal form: $\Lambda(\theta) = \mathrm{blockdiag}(\mathrm{Id}, \Lambda_N(\theta))$. Then, using this methodology, it is easy to separate the Lyapunov multipliers corresponding to tangent directions to the torus, which are all equal to 1, from the ones corresponding to normal directions, which are assumed to be different from 1 (as long as the torus is normally hyperbolic). The analysis of the normal linearized dynamics, given by the linear skew-product (Λ_N, R_ω), is in order. For instance, its Lyapunov multipliers can be computed by using QR methods, or, specially for low dimension (as in the examples of this paper, with $n = 2$), using variants of power method. However, when using reducibility methods, the matrix Λ_N is constant and the Lyapunov multipliers are just the moduli of its eigenvalues, so there is no need of separate algorithms for the computation of the eigenvalues. (For reducibility, we assume that ω is Diophantine).

It is well known that, in virtue of Oseledets theorem, vectors associated with Lyapunov multipliers appear in measurable invariant bundles, the so-called *Lyapunov bundles*. The Lyapunov bundles corresponding to the Lyapunov multipliers smaller than 1 span the stable bundle N^s, while the ones corresponding to Lyapunov multipliers greater than 1 span the unstable bundle N^u. Both the stable and unstable bundles of a normally hyperbolic invariant torus are smooth (and in this paper, even real-analytic). The algorithm based on hyperbolic block-diagonalizability produces these bundles. Hence, in order to measure the quality of the normal hyperbolicity, we will consider not only the normal Lyapunov multipliers (that should be far from 1), but also the angles between tangent, stable and unstable subbundles (Calleja and Figueras 2012; Haro and de la Llave 2006a, 2007). The quality of the reducibility properties of dynamics in stable and unstable bundles is also measured by the angles between the Lyapunov bundles spanning them.

In the examples of this paper, the dimensions are $d = 1, n = 2$. So, we will focus the discussion in this case. Let $\chi_1 = 1$ be the Lyapunov multiplier corresponding to the tangent bundle L, and χ_2, χ_3 be the Lyapunov multipliers corresponding to the normal invariant bundle N. We will denote by α_{LN} the infimum angle between the tangent

and the invariant normal bundle, which is strictly positive if the torus is normally hyperbolic. We also define, for $i \neq j$, α_{ij} as the infimum angle between Lyapunov bundles of χ_i and χ_j. These angles are strictly positive when the corresponding bundles are continuous. The dynamics on the tangent bundle is reduced to multiply by 1, i.e. the linear skew-product has an eigenvalue $\lambda_1 = 1$. We are also interested in reducibility properties of the invariant normal bundle, which is isomorphic to $\mathbb{R}^2 \times \mathbb{T}$. Then, we find the following classification for a quasi-periodic normally hyperbolic invariant torus:

- If $\chi_2 < \chi_3 < 1$ (resp. $1 < \chi_3 < \chi_2$), the torus is attracting (resp. repelling). The Lyapunov bundle associated with χ_2 is the fast stable (resp. unstable) bundle, and the one associated to χ_3 is the slow stable (resp. unstable) bundle.
  - In the reducible case, the torus is an attracting (resp. repelling) node torus. The fast and slow stable (resp. unstable) bundles are continuous, and in fact as smooth as the cocycle. The eigenvalues of the constant matrix Λ_N are $\lambda_2, \lambda_3 \in \mathbb{R}$, so that $|\lambda_2| = \chi_2$ and $|\lambda_3| = \chi_3$. The angle α_{23} is positive. We can define a topological index for both bundles, as subbundles of the invariant normal bundle.
  - In the non-reducible case, the torus is a non-reducible attracting (resp. repelling) torus. The fast and slow stable (resp. unstable) bundles are measurable but not continuous. We cannot assign signs to the Lyapunov multipliers (since no eigenvalues can be defined), and we will write $\lambda_2 = \pm\chi_2$ and $\lambda_3 = \pm\chi_3$. The angle α_{23} is zero.
- If $\chi_2 = \chi_3 < 1$ (resp. $1 < \chi_3 = \chi_2$), the torus is attracting (resp. repelling).
  - In the reducible case, the eigenvalues λ_2 and λ_3 of the constant matrix Λ_N have the same modulus, so $|\lambda_2| = |\lambda_3|$. Either both are real, and the torus is an attracting (resp. repelling) degenerate node torus, or complex conjugate, and the torus is an attracting (resp. repelling) focus torus. By convection, we take angle $\alpha_{23} = 0$ in this case. The argument of the eigenvalues is the rotation number of the cocycle (Λ_N, R_ω).
  - In the non-reducible case, one cannot define eigenvalues.
- If $\chi_2 < 1 < \chi_3$ the torus is of saddle type. A saddle torus is reducible, and the eigenvalues of the constant matrix Λ_N are $\lambda_2, \lambda_3 \in \mathbb{R}$, so that $|\lambda_2| = \chi_2$, $|\lambda_3| = \chi_3$. The angle α_{23} is positive. We can define a topological index for the stable and unstable bundles, as subbundles of the invariant normal bundle.

In a continuation of a torus with respect to a parameter, say ε, monitoring the Lyapunov multipliers close to 1 is useful to detect quasi-periodic bifurcations, while monitoring the angles between tangent, stable, unstable bundles, and the internal Lyapunov bundles, are useful to detect bundle collisions and breakdowns.

We emphasize that node and saddle types are open conditions in the parameter space, while focus and non-reducible types are closed conditions that happen in Cantor sets of positive measure in the parameter space. A typical and well-understood phenomenon is the transition from a node torus to a focus torus. This corresponds to the coincidence of the real eigenvalues at a certain critical parameter, while their corresponding fast and slow bundles uniformly collide. At the moment of this collision, the torus is a degenerate node torus, and after the critical value the torus is of focus type. Another

feature of this phenomenon is that the angle between the slow and fast bundles behaves as an square root when the parameter ε goes to the critical collision parameter ε_c: $\alpha_{23}(\varepsilon) \sim A(\varepsilon_c - \varepsilon)^{\frac{1}{2}}$. We describe this transition in Sect. 6. A much less known phenomenon is when the fast and slow bundles of a node torus collide although the Lyapunov multipliers remain separated (Jalnine and Osbaldestin 2005; Haro and de la Llave 2006a). This collision is non-uniform and the bundles go from being smooth to being measurable. This bundle merging scenario corresponds to a loss of reducibility in the normal dynamics, but does not imply the immediate destruction of the torus. Moreover, one observes that, in contrast with the previous transition, in this case $\alpha_{23}(\varepsilon) \sim A(\varepsilon_c - \varepsilon)$, a conjecture that in Haro and de la Llave (2006a) was stated in the context of quasi-periodically forced systems and that was rigorously proved in specific cases in Bjerklöv and Saprykina (2008). We report on the appearance of this transition in the context of this paper in Sect. 7.

In the previous circumstances, the Lyapunov multipliers in the normal directions were far from 1 and the angle between the tangent and the invariant normal bundles were bounded from zero, so neither torus bifurcations nor torus breakdowns were produced along the transitions (but could result in new phenomena when tuning further parameter ε). Classical bifurcations have their counterparts in quasi-periodic bifurcation theory (see e.g. Broer et al. 1990; Chenciner and Iooss 1979a, b). For instance, if in a continuation of a node or a saddle torus we have $\chi_3 \to 1$ as $\varepsilon \to \varepsilon_c$, then if $\lambda_3 \to 1$, the generic case is a quasi-periodic saddle-node bifurcation, while if $\lambda_3 \to -1$, the generic case is a quasi-periodic period doubling bifurcation. A typical bifurcation of focus tori is the quasi-periodic Hopf bifurcation, in which $\chi_2 = \chi_3 \to 1$ as $\varepsilon \to \varepsilon_c$, and the corresponding eigenvalues cross the unit circle (under appropriate non-resonant conditions). The key word here is reducibility, so these quasi-periodic bifurcations are well understood. Notice that in these bifurcations the angle between the tangent and the invariant normal bundles α_{LN} is bounded from zero. The situation if the angle α_{LN} goes to zero at a critical parameter ε_c, while the normal Lyapunov multipliers remain far from 1, is dramatically different to the classical quasi-periodic bifurcations. In this case, the condition of normal hyperbolicity is becoming more deteriorated not because the rates of growth in the normal directions stop dominating those in the tangent directions, but because the tangent and invariant normal bundles approach each other (in a non-uniform way). Hence, this bundle merging scenario produces the breakdown of the torus (see Calleja and Figueras 2012 for the description of the phenomenon for attracting invariant tori in conformally symplectic systems). We report in Sects. 5 and 6 on such behavior in a saddle torus and in an attracting node torus, respectively. In particular, our findings lead to the following conjecture, that complement Conjecture 4.1.

Conjecture 4.4 *Let $F_{a,\varepsilon} : \mathbb{T} \times \mathbb{R}^n \to \mathbb{T} \times \mathbb{R}^n$ be a family of real-analytic maps, where a is the adjusting parameter and ε is the continuation parameter. Let $(K_\varepsilon, a_\varepsilon)$ be a family of quasi-periodic normally hyperbolic invariant tori parameterized by $K_\varepsilon : \mathbb{T} \to \mathbb{T} \times \mathbb{R}^n$ and their adjusting parameters, where $\varepsilon \in [0, \varepsilon_c[$. Then, when the torus breaks down in a bundle merging scenario at a critical value ε_c, the angle between the tangent and the invariant normal bundles goes to zero as*

$$\alpha_{LN}(\varepsilon) \sim A(\varepsilon_c - \varepsilon),$$

when $\varepsilon \to \varepsilon_c$.

The previous conjecture deals with the immediate breakdown of a torus when the reducibility is lost because the tangent bundle and the invariant normal bundle non-uniformly collide. As we have mentioned above, the dynamics in the invariant normal bundle can also lose the reducibility property, a phenomenon that does not imply the immediate breakdown of the torus but that could be its cause if the less dominant normal Lyapunov multiplier goes to 1 when varying parameter ε. Such a phenomenon is reported in Sect. 7.

5 On the Continuation of a Saddle Torus up to Its Breakdown in a Conservative System

In this section, we perform a continuation of a quasi-periodic saddle torus, with golden mean frequency ω, for the 3D-FAF (29), with parameters $b = 0.25$, $c = 4$. Then, since $bc = 1$, the map is volume preserving. The continuation starts at $\varepsilon = 0$, for which one can determine in an explicit way the invariant torus and the invariant bundles by paper and pencil computations. In particular, $a(0) = \omega$. Since we continue saddle tori and their bundles are 1-dimensional, it is natural to use the algorithm based on complete reducibility, see Sect. 3.3.3. Hence, along the continuation we compute the eigenvalues $\lambda_S = \lambda_2$ and $\lambda_U = \lambda_3$ of the associated cocycle (with $\lambda_S\lambda_U = 1$), as well as we monitor the angles between the invariant bundles $\alpha_{LS} = \alpha_{12}, \alpha_{LU} = \alpha_{13}, \alpha_{SU} = \alpha_{23}$. The results are displayed in Table 2. See also Fig. 2 for some quasi-periodic saddle tori and the angles between the tangent, stable, and unstable subbundles, spanned by L, N^S and N^U, respectively.

When increasing parameter ε, the torus and its bundles are becoming more irregular, and the implementation of the algorithm adapts the number of Fourier modes of the approximations up to $N_F = 1{,}048{,}576$, the limiting number of Fourier modes in our implementations. This is an indication that the torus is about to break at a certain param-

Table 2 Continuation of a saddle torus with respect to ε: continuation parameter, adjusting parameter, eigenvalues of the linearized equation and angles between bundles

ε	a	λ_S	λ_U	α_{LS}	α_{LU}	α_{SU}
0.000000	3.8832220775	0.2500000000	4.0000000000	1.23529e+00	9.67700e−01	7.53151e−01
1.000000	3.8765074834	0.2470073613	4.0484623406	5.84550e−01	7.24296e−01	4.74488e−01
1.900000	3.8627251961	0.2360025603	4.2372421662	4.06820e−02	4.85572e−01	4.55743e−01
1.980000	3.8612901228	0.2341969934	4.2699096403	1.58441e−03	4.64434e−01	4.60560e−01
1.983000	3.8612358919	0.2341236575	4.2712471286	1.48398e−04	4.63643e−01	4.60725e−01
1.983200	3.8612322755	0.2341187477	4.2713367041	5.26130e−05	4.63591e−01	4.60736e−01
1.983210	3.8612320947	0.2341185021	4.2713411844	4.78291e−05	4.63588e−01	4.60736e−01
1.983211	3.8612320766	0.2341184775	4.2713416324	4.73511e−05	4.63588e−01	4.60736e−01

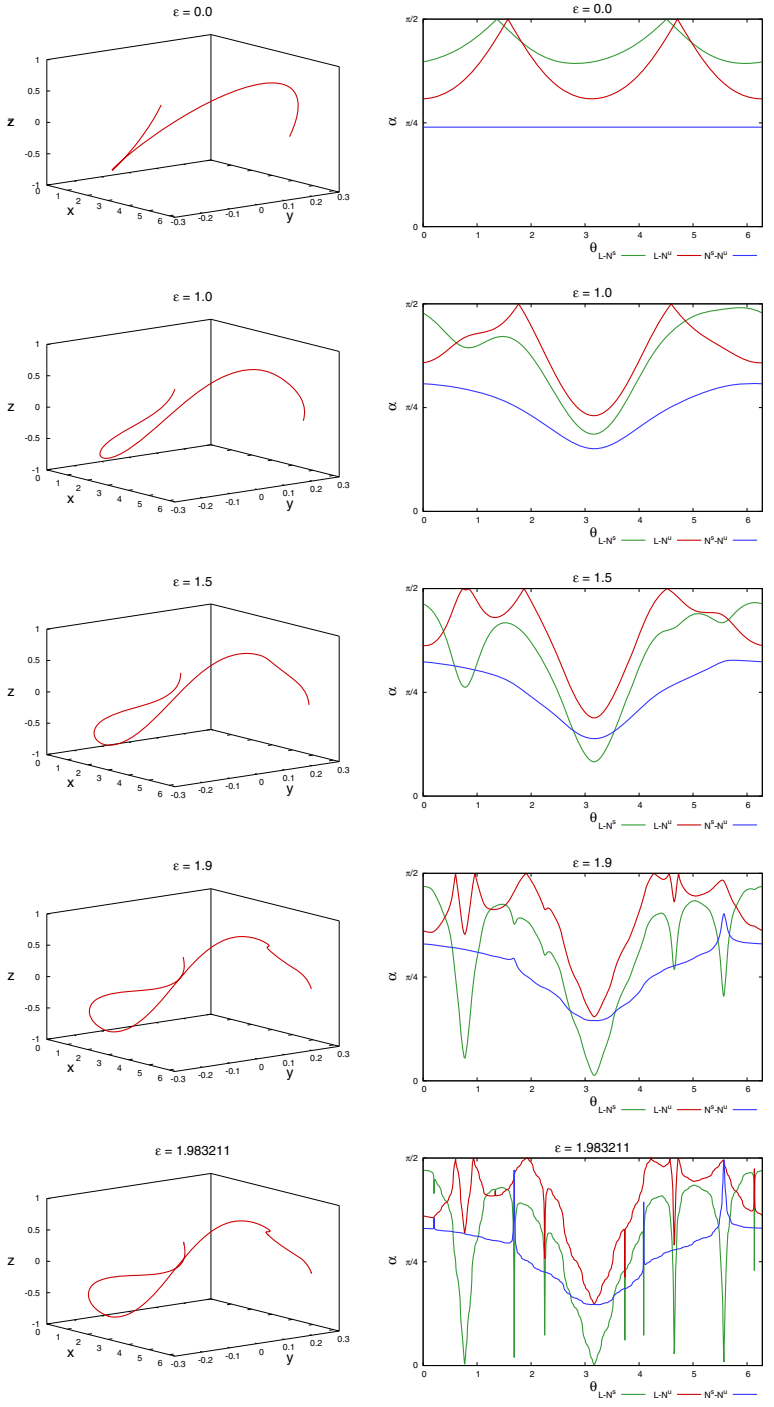

Fig. 2 Continuation of a saddle torus with respect to ε: invariant tori (*left*) and angles between bundles (*right*)

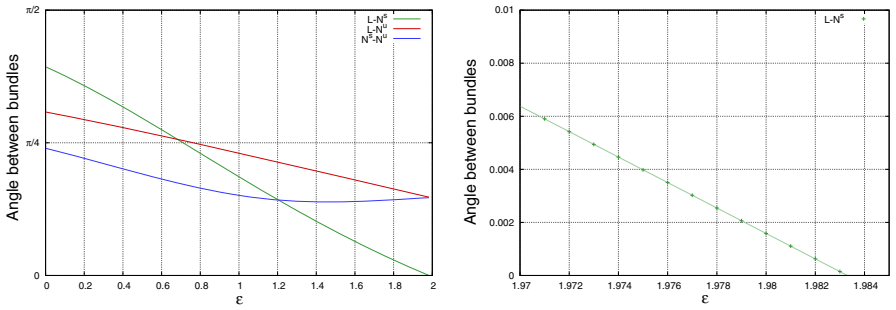

Fig. 3 Continuation of a saddle torus with respect to ε: angles between bundles. *Left* angle between bundles with respect to ε. *Right* α_{LS} close to the breakdown

eter ε_c. The explanation of this behavior is provided by the dynamical observables, from which we study how the properties of normal hyperbolicity of the torus deteriorate. From Table 2, we observe that, in some sense, hyperbolicity properties improve since stable and unstable Lyapunov multipliers ($\chi_S = |\lambda_S|$ and $\chi_U = |\lambda_U|$) move apart from the tangent Lyapunov multiplier ($\chi_1 = 1$), but they become more non-uniform since the angle α_{LN} between the tangent and the invariant normal bundles goes to zero. In fact, what we observe in this example is that the angle α_{LS} between the tangent and stable bundles goes to zero, while the angle α_{LU} between the tangent and unstable bundles is far from zero. We refer to this phenomenon as to a *bundle merging scenario* between the tangent and the stable bundles, which collide non-smoothly, causing the destruction of the saddle torus. Near the breakdown, we observe a linear decay to zero of the angle between the tangent and stable bundle, given by the expression

$$\alpha_{LS}(\varepsilon) \simeq 0.95101870 - 0.47951222\,\varepsilon.$$

The fit over the last 10 values of the continuation process appears in Fig. 3 (right), which supports Conjecture 4.4. From this fit, we can extrapolate an approximation of the critical breakdown value ε_c by solving $\alpha_{LS} = 0$:

$$\varepsilon_{c,LS} \simeq 1.98330439.$$

Another indicator of the breakdown of a torus is the blow up of Sobolev and C^r seminorms at the critical parameter ε_c. Table 3 and Fig. 4 illustrate this behavior in the present example, for the H^2 and C^1 seminorms (the critical parameter is labeled with a blue vertical line). In particular, the asymptotic behavior of the H^2 and C^1 seminorms is given by the following expressions:

$$H^2(\varepsilon) \simeq \frac{0.52106152}{(1.98331250 - \varepsilon)^{1.03657369}}, \quad C^1(\varepsilon) \simeq \frac{1.36754056}{(1.98333604 - \varepsilon)^{0.47751520}}.$$

Then, the corresponding critical values for the critical parameter of breakdown are

Table 3 Continuation of a saddle torus with respect to ε: H^2 and C^1 seminorms, and number of Fourier modes

ε	H^2	C^1	N_F
0.000000	0.00000e+00	0.00000e+00	64
1.000000	3.93198e−01	4.51560e−01	64
1.900000	9.25609e+00	4.02912e+00	1024
1.980000	2.74229e+02	2.08560e+01	16384
1.983000	3.16805e+03	6.23433e+01	131,072
1.983200	9.23013e+03	9.98547e+01	524288
1.983210	1.01840e+04	1.04263e+02	1,048,576
1.983211	1.02901e+04	1.04738e+02	1,048,576

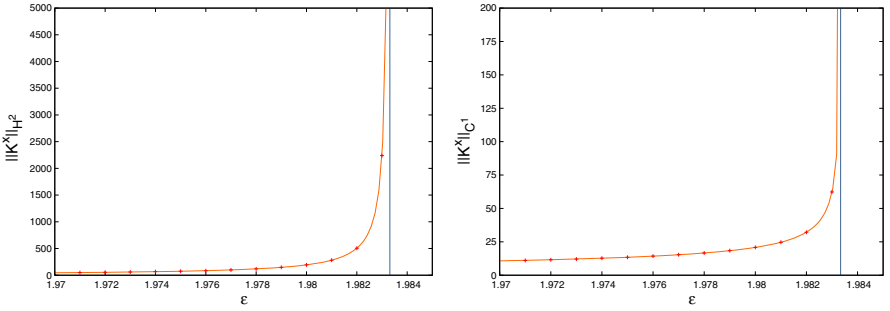

Fig. 4 Continuation of a saddle torus with respect to ε: blow up of H^2 and C^1 seminorms

$$\varepsilon_{c,H^2} \simeq 1.98331250, \quad \varepsilon_{c,C^1} \simeq 1.98333604,$$

which coincide up to five significant digits with the critical value $\varepsilon_{c,LS}$, and the critical exponents are

$$B_2 \simeq 1.03657369, \quad \hat{B}_1 \simeq 0.47751520.$$

This blow up of the seminorms supports our assertions in Conjecture 4.1.

We have also computed the blow up for different H^r and C^r seminorms (with $r \in [0, 4]$), obtaining their corresponding estimates ε_{c,H^r} and ε_{c,C^r} of the critical parameter ε_c of the breakdown, and their critical exponents B_r and $\hat{B}_r$. The results are displayed in Table 4. The behavior of the critical exponents supports Conjecture 4.1, since they satisfy

$$\begin{aligned} B_r &\simeq -0.86158681 + 0.94921635\, r, \quad \text{for } r \geq r_c \simeq 0.90768225, \\ \hat{B}_r &\simeq -0.46503572 + 0.93164713\, r, \quad \text{for } r \geq \hat{r}_c \simeq 0.49915435, \end{aligned}$$

respectively. See also Fig. 5. Incidentally, we obtain the critical regularities in Sobolev and C^r spaces. Notice that these approximations of the critical exponents fit better in the range $r \in [1.5, 2.5]$ for Sobolev seminorms and, in the range $r \in [1, 2]$ for C^r seminorms, see Table 4. If the Sobolev or C^r range is smaller than the corresponding

Table 4 Estimates of the critical value ε_c of the breakdown of the saddle torus and the critical exponent, for the Sobolev and C^r seminorms, respectively

r	ε_{c,H^r}	B_r	ε_{c,C^r}	$\hat{B}_r$
0.0	2.3659464613	0.2923785848	1.9990850327	0.0297868131
0.2	2.0586744062	0.0813569806	1.9861547446	0.0307922402
0.4	2.0004005665	0.0384265744	1.9837333445	0.0993803809
0.6	1.9871411293	0.0355595795	1.9834952022	0.2004862355
0.8	1.9840987055	0.0631748194	1.9833823470	0.3248803775
1.0	1.9834618324	0.1454271549	1.9833360406	0.4775151988
1.2	1.9833384372	0.2908069846	1.9833190481	0.6502075333
1.4	1.9833176436	0.4695009290	1.9833138158	0.8337511825
1.6	1.9833139955	0.6572301080	1.9833131090	1.0221473834
1.8	1.9833129682	0.8467031525	1.9833145987	1.2125264852
2.0	1.9833125000	1.0365736863	1.9833139383	1.4048686885
2.2	1.9833122392	1.2266035739	1.9833066911	1.5878751888
2.4	1.9833120811	1.4167235069	1.9833093694	1.7800335253
2.6	1.9833119793	1.6068996870	1.9833107898	1.9717868183
2.8	1.9833119103	1.7971125472	1.9833114583	2.1630388912
3.0	1.9833118614	1.9873500514	1.9833118090	2.3540487329
3.2	1.9833118254	2.1776042766	1.9833119188	2.5448764649
3.4	1.9833117977	2.3678696152	1.9833116434	2.7352870374
3.6	1.9833117758	2.5581420338	1.9833107989	2.9247764069
3.8	1.9833117582	2.7484190289	1.9833090236	3.1123520542
4.0	1.9833117441	2.9386999211	1.9833137278	3.3135418818

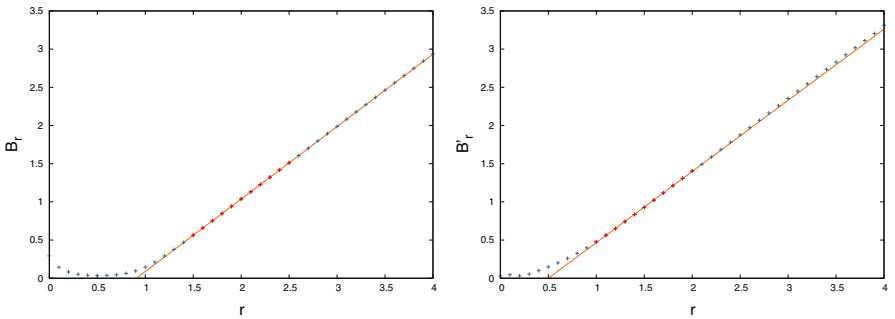

Fig. 5 Fit for the affine expression of the critical exponents for the saddle torus, given by expressions (37) and (36) of Conjecture 4.1, that is B_r and $\hat{B}_r$ (labeled as B'_r in this picture), respectively

regularity of the invariant curve, the associated norms do not explode and there are not critical exponents. On the other side, if the range is too high, then there are numerical instabilities in the computation of the Sobolev and C^r norms, since the high-order Fourier coefficients are multiplied by very big weights.

6 On Node-Focus Transitions in the Continuation of an Attracting Torus up to Its Breakdown in a Dissipative System

In this section, we consider the 3D-FAF (29) with parameters $b = 0.5$ and $c = 0.4$. Then, since $bc = 0.2$, the map is dissipative. We continue an attracting quasi-periodic invariant torus with frequency the golden mean, and its 2-dimensional stable bundle, from parameter $\varepsilon = 0$. In particular, for $\varepsilon = 0$ we can use the same expressions we used for the initial approximations in Sect. 5, where the eigenvalues of Λ_N are 0.5 and 0.4. It is then natural to use the algorithm based on complete reducibility, see Sect. 3.3.3, so that we compute the attracting node torus and the slow and fast invariant bundles (N^S and N^{SS}), their eigenvalues ($\lambda_S = \lambda_3$ and $\lambda_{SS} = \lambda_2$), and the angles between bundles (α_{LN} and $\alpha_{SS} = \alpha_{23}$). See Table 5 and Fig. 6.

The algorithm based on complete reducibility detects when this reducibility property fails, and the dynamical observables provide an explanation of the failure. In the present example, the real eigenvalues collide at a critical parameter

$$\varepsilon_{\mathrm{A}} \simeq 0.61129562,$$

Table 5 Continuation of an attracting node torus with respect to ε by using the complete reducibility algorithm: continuation parameter, adjusting parameter, eigenvalues of the linearized equation and angles between bundles

ε	a	$\lambda_{SS} = \lambda_2$	$\lambda_S = \lambda_3$	$\alpha_{SS} = \alpha_{23}$
0.0000000000	3.8832220775	0.4000000000	0.5000000000	2.44979e−01
0.2000000000	3.8825174896	0.4020837925	0.4974087583	2.31429e−01
0.4000000000	3.8805105878	0.4096616727	0.4882077414	2.15809e−01
0.6000000000	3.8773582471	0.4367863921	0.4578897228	5.83418e−02
0.6100000000	3.8771703292	0.4436248363	0.4508313858	1.98262e−02
0.6110000000	3.8771513697	0.4454942403	0.4489395858	9.47391e−03
0.6112812500	3.8771460318	0.4468334169	0.4475940968	2.09229e−03
0.6112956166	3.8771457591	0.4472071096	0.4472200814	3.67750e−05

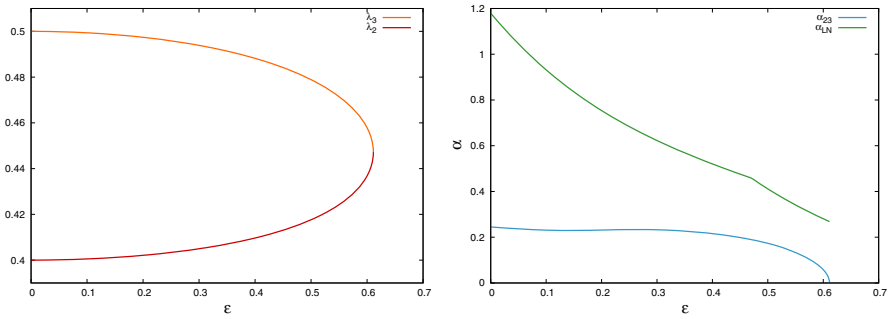

Fig. 6 Continuation of an attracting node torus with respect to ε by using the complete reducibility algorithm. *Left* eigenvalues of the linearized equation. *Right* angle between bundles

and the distance between the fast and slow stable bundles goes to zero at a square root rate. The collision of the eigenvalues at ε_A coincides with the smooth collision between the fast and slow stable bundles. Notice that the tangent and the stable bundles remain separated in this transition.

At ε_A there is a node-focus transition, after which the torus is reducible, but not completely reducible. The torus is then of focus type: the eigenvalues λ_2, λ_3 of Λ_N are complex conjugated. In this situation, we can use the algorithm based on reducibility, see Sect. 3.3.2, to keep going with the continuation process of the torus and its eigenvalues. In the continuation process, normal resonances (the failure of the second Melnikov condition) play an important role. For instance, a sufficiently large step size permits to cross those resonances. In our example, a small step size $\Delta\varepsilon = 10^{-3}$ makes the algorithm to stop at $\varepsilon_B \simeq 0.77660160$, while with larger step size $\Delta\varepsilon = 10^{-1}$ the algorithm continues till $\varepsilon_D \simeq 0.88354197$. These parameter values correspond to resonances leading to focus-node transitions, in which the tori are again of attracting node type. We emphasize that the topology of the fast and slow stable bundles could be non-trivial, and they could be non-orientable. These problems can be overcome by detecting normal resonances and recomputing the adapted frame to fit the invariant bundles, and, in case these bundles are non-orientable, using tricks as performing double covering (Haro and de la Llave 2007).

Instead of using the previous reducibility methods, we illustrate here the performance of the algorithm based on hyperbolic block-diagonalizability, described in Sect. 3.3.1. An advantage of the method is that it goes through all the changes of the dynamical properties in the normal directions, and a drawback is that dynamical information as Lyapunov multipliers and their associated bundles has to be computed apart. Figure 7 shows several invariant tori and the corresponding (projectivized) slow and fast bundles. With this algorithm, the continuation process crosses node-focus transitions. In Fig. 8 we observe several resonances, some of which have been magnified in Fig. 9. To the previously computed node-focus transitions and ε_B, ε_D, we add, for instance, the ones at $\varepsilon_F \simeq 0.96631953$ and $\varepsilon_H \simeq 0.97849103$. We recall that resonances, that correspond to tori of node type, appear in open sets of the space of parameters, while tori of focus type appear in a Cantor set of parameters. See e.g. Jorba and Simó (1992, 1996).

In order to analyze the dynamics and topology changes in resonances, we compute the slow and fast stable bundles of the node tori (gray rows in Table 6) as invariant bundles of the normal cocycle (Λ_N, R_ω), the corresponding indices, and we assign signs to the Lyapunov multipliers in order to obtain the eigenvalues of the torus. See Table 6. Both the slow and fast stable bundles can be computed applying the power method (either forward or backwards) to the normal cocycle. We can compute the corresponding indices by counting the number of turns of the bundles. This number is the index

$$\frac{m}{2} = \frac{\beta}{2\pi},$$

where β is the total angle the bundle runs when θ, the parameter on the torus, goes from 0 to 2π. Both bundles have the same index. If the double-index m is even, then

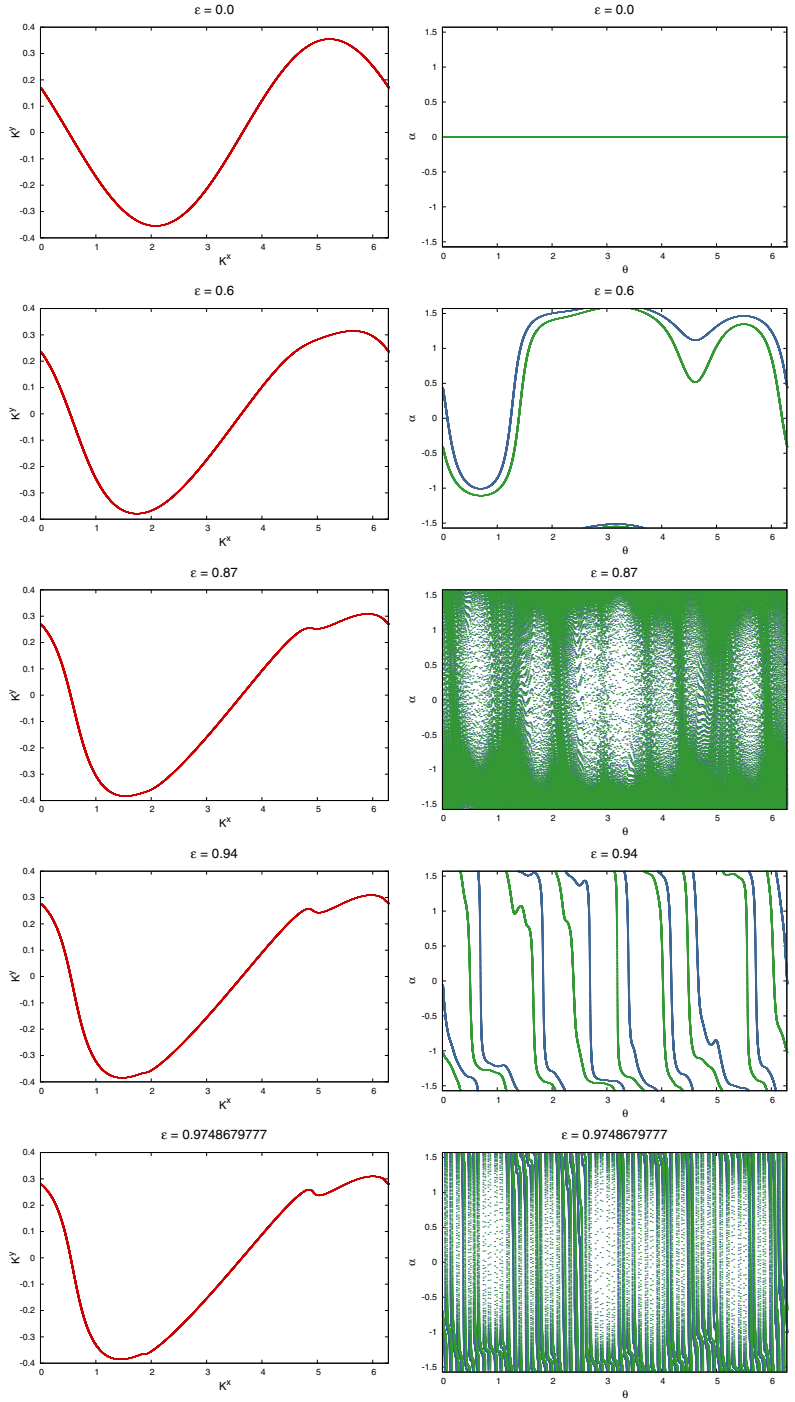

Fig. 7 Continuation of an attracting torus with respect to ε: (x,y)-projection of invariant tori (*left*) and angles of slow and fast bundles with respect to the horizontal axis (*right*)

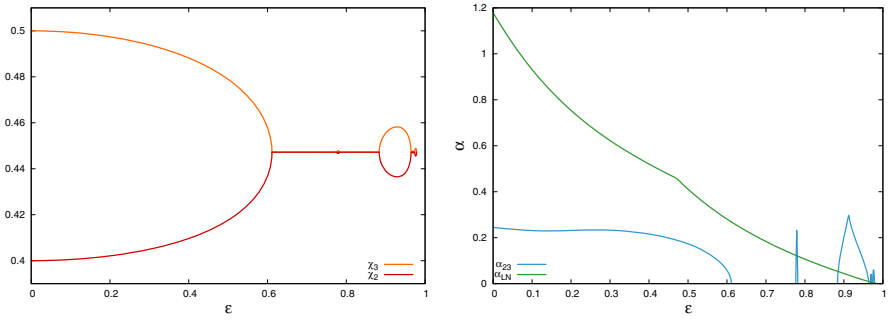

Fig. 8 Continuation of an attracting torus with respect to ε by using the hyperbolic block-diagonalizability algorithm. *Left* Lyapunov multipliers. *Right* angles between bundles

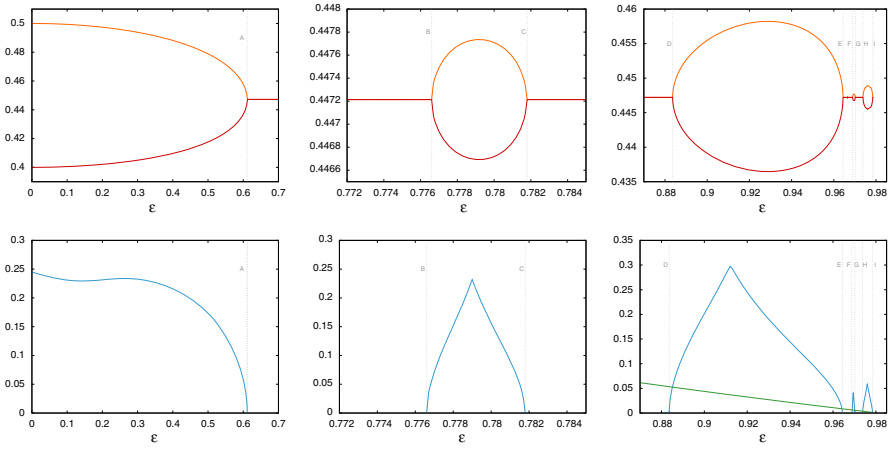

Fig. 9 Continuation of an attracting torus with respect to ε by using the hyperbolic block-diagonalizability algorithm: magnifications of Lyapunov multipliers (*top*) and angle between bundles (*down*) around several resonances

the bundle is orientable, whereas if m is odd, the bundle is non-orientable. Moreover, the sign of m gives the direction that the fiber rotates, either counterclockwise $(+)$ or clockwise $(-)$. See the last column in Table 6. The parameters of this table marked in bold correspond to the pictures in Fig. 7. In particular, $\varepsilon = 0.0$ and 0.6 correspond to node tori with orientable bundles of index 0; $\varepsilon = 0.87$ corresponds to a *focus torus*; and $\varepsilon = 0.94$ and 0.97486798 correspond to node tori with orientable bundles with index -4, and non-orientable bundles with index $\frac{-63}{2}$, respectively. In order to assign a sign to the eigenvalues, notice that each subbundle of $\mathbb{T} \times \mathbb{R}^2$ can be represented by two curves in $\mathbb{T} \times \mathbb{S}^1$ (or a single curve in $\mathbb{T} \times \mathbb{P}^1$, as in Fig. 7). Then, if each of the curves is fixed under iteration of the normal cocycle, we assign a positive sign to the eigenvalue. Otherwise, if the copy is 2-periodic, that is, it is shipped to the other copy, we assign a negative sign. Of course, the main assumption here is that the torus is of node type, so the bundles are continuous. When the torus is of focus type (white rows in Table 6) the eigenvalues are complex conjugated, the Lyapunov multipliers are

Table 6 Continuation of an attracting torus with respect to ε by using the hyperbolic block-diagonalizability algorithm: continuation parameter, adjusting parameter, eigenvalues of the linearized equation, angle between bundles and index of the bundles

ε	a	λ_2	λ_3	α_{LN}	index×2
0.0000000000	3.8832220775	0.4000000000	0.5000000000	1.17932e+00	0
0.6000000000	3.8773582471	0.4367722458	0.4579030644	2.80952e-01	0
0.6112956166	3.8771457591	0.4472071096	0.4472200814	2.68560e-01	0
0.6500000000	3.8763877719	$\lvert\cdot\rvert \simeq 0.4472135955$		2.28944e-01	–
0.7000000000	3.8753378014			1.83379e-01	
0.7780000000	3.8735326319	0.4467502443	0.4476774260	1.20776e-01	13
0.7810000000	3.8734589788	0.4468415827	0.4475859170	1.20060e-01	13
0.8000000000	3.8729849911	$\lvert\cdot\rvert \simeq 0.4472135955$		1.06723e-01	–
0.8700000000	3.8711212578			6.15360e-02	
0.9000000000	3.8702618736	–0.4390977148	–0.4554795000	4.38126e-02	– 8
0.9400000000	3.8690546139	–0.4369038657	–0.4577666206	2.14837e-02	– 8
0.9650000000	3.8682620624	$\lvert\cdot\rvert \simeq 0.4472135955$		8.21239e-03	–
0.9660000000	3.8682297243			7.69179e-03	
0.9664195313	3.8682161425	0.4471829177	0.4472442872	7.47361e-03	–152
0.9665195313	3.8682129039	0.4471254316	0.4473017886	7.42163e-03	–152
0.9670000000	3.8681973361	$\lvert\cdot\rvert \simeq 0.4472135955$		7.17195e-03	–
0.9680000000	3.8681648979			6.65290e-03	
0.9690000000	3.8681324095	0.4470641148	0.4473631379	6.13459e-03	81
0.9700597656	3.8680979246	0.4469783005	0.4474490260	5.58617e-03	81
0.9702000000	3.8680933571	$\lvert\cdot\rvert \simeq 0.4472135955$		5.51366e-03	–
0.9725000000	3.8680183043			4.32655e-03	
0.9738288651	3.8679748195	–0.4471093093	–0.4473179175	3.64248e-03	–63
0.9748679777	3.8679407539	–0.4458282085	–0.4486032989	3.10852e-03	–63
0.9761123718	3.8678998859	–0.4455276098	–0.4489059727	2.47015e-03	–63
0.9787153549	3.8678141438	$\lvert\cdot\rvert \simeq 0.4472135955$		1.13849e-03	

In bold it appears the ε parameter values corresponding to pictures in Fig. 7

equal, and the stable bundle can not split in a direct sum of (real) invariant continuous subbundles.

To conclude the study of this example, we consider now the mechanism of breakdown of the invariant torus. We observe that the angle α_{LN} between the tangent and the stable bundle tends to zero (see the green curve in Fig. 8, left and Table 6), while the normal Lyapunov multipliers remain far from 1 (Fig. 8, right). This behavior indicates that there is a collision between the tangent and the stable bundles that destroys the invariant torus at a critical breakdown parameter ε_c. This mechanism of breakdown is again a bundle merging scenario as in Sect. 5, but in this case the stable bundle is 2-dimensional. Moreover, there is a linear decay to zero given by the expression

$$\alpha_{LN}(\varepsilon) \simeq 0.51022350 - 0.52017767\ \varepsilon$$

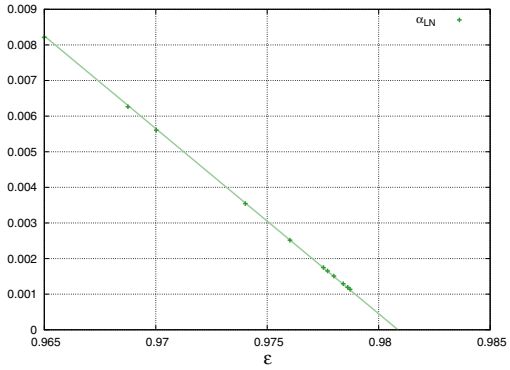

Fig. 10 Continuation of an attracting torus with respect to ε: α_{LN} close to breakdown

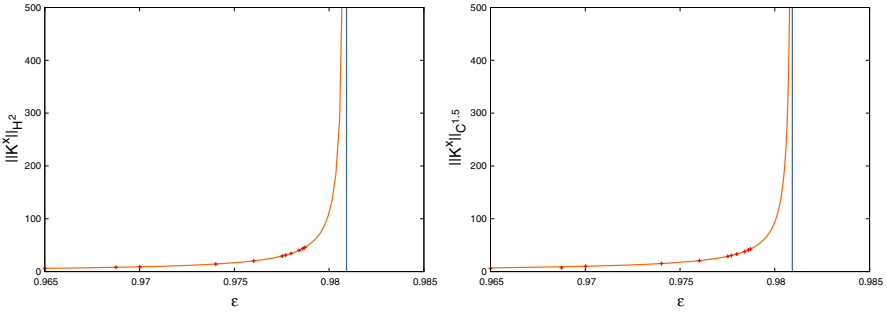

Fig. 11 Continuation of an attractor torus with respect to ε: blow up of H^2 and $C^{1.5}$ seminorms (critical value labeled with a *blue line*) (Color figure online)

supporting Conjecture 4.4, from which we extrapolate an approximation

$$\varepsilon_{c,LN} \simeq 0.98086389$$

of ε_c (see Fig. 10). We also compute the H^2 and $C^{1.5}$ seminorms of the torus, which at the critical value ε_c blows up as

$$H^2(\varepsilon) \simeq \frac{0.08998717}{(0.98091680-\varepsilon)^{1.01837794}}, \quad C^{1.5}(\varepsilon) \simeq \frac{0.16768158}{(0.98092418-\varepsilon)^{0.90596220}}.$$

providing a new estimate

$$\varepsilon_{c,H^2} \simeq 0.98091680, \quad \varepsilon_{c,C^{1.5}} \simeq 0.98092418,$$

of ε_c. Notice that, even though the last computed torus (that is of focus type), $\varepsilon = 0.9787153549$, is not extremely close to the breakdown, both estimates $\varepsilon_{c,LN}$, ε_{c,H^2} and $\varepsilon_{c,C^{1.5}}$ differ in the fifth digit. See Fig. 11 for the results.

Moreover, to get information about the regularity of the torus at the breakdown, we compute the linear expression of the critical exponents for different H^r and C^r seminorms, given by Conjecture (4.1):

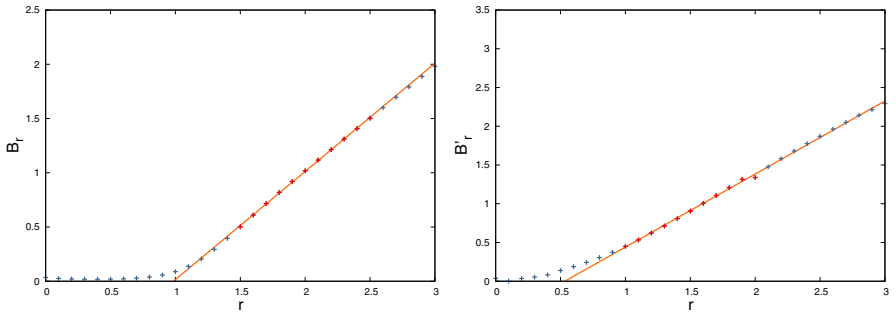

Fig. 12 Fit for the affine expression of the critical exponents for the attracting torus, given by expressions (36) and (37) of Conjecture 4.1, that is B_r and $\hat{B}_r$ (labeled as B'_r in this picture), respectively

$$B_r \simeq -0.98252283 + 0.99740066\, r,$$
$$\hat{B}_r \simeq -0.50195007 + 0.94279767\, r,$$

respectively. In particular, the H^r seminorms explode for values $r \geq r_c \simeq 0.985083$ and the C^r seminorms for $r \geq \hat{r}_c \simeq 0.532405$. See Fig. 12.

7 On the Fractalization of an Attracting Torus

In this section, we consider the 3D-FHF (30) with parameters $b = 0.68, c = 0.1$, and $d = 1$. The case $d = 0$, that corresponds to a quasi-periodically forced dynamical system, has been considered in Sosnovtseva et al. (1996), Haro and de la Llave (2006a, 2007). The quasi-periodic arcs of the continuation of a torus with frequency ω, corresponding to $d = 0$ and $d = 1$, are shown in Fig. 1b. We discuss below the case $d = 1$.

When $\varepsilon = 0$, the family (30) is a direct product of a rotation by angle a and the classical Hénon map. Hence, the torus parameterized by $K_0(\theta) = (\theta, y_0, z_0)$, with $y_0 = \frac{1}{2b}\left(c - 1 + \sqrt{(c-1)^2 + 4b}\right)$ and $z_0 = cy_0$, is a saddle torus, and its internal dynamics is the rotation R_ω by choosing $a = \omega$. We also have straightforward formulas for the stable and unstable bundles and their eigenvalues λ_2 and λ_3, respectively.

In a leading continuation, we use the algorithms based on reducibility to continue the torus with respect to the perturbation parameter ε, as well as the adjusting parameter, a, and the eigenvalues of the linearized normal dynamics, λ_2, λ_3, which is reduced to a constant cocycle. Recall that the Lyapunov multipliers are $\chi_2 = |\lambda_2|$ and $\chi_3 = |\lambda_3|$. The results are displayed in Table 7. We observe two phenomena related with the dynamics in the invariant normal bundle described by the cocycle (Λ_N, R_ω). The first phenomenon is a subcritical period-doubled bifurcation of the saddle torus at $\varepsilon_A \lesssim 0.26$, after which the torus is an attracting node torus. Notice that, even though the eigenvalue λ_3 crosses -1, and so the maximal Lyapunov multiplier crosses 1, the continuation jumps the critical bifurcation value ε_A, in which the torus is not normally hyperbolic. The stable and unstable bundles before the bifurcation become the fast and slow stable bundles, respectively, after the bifurcation.

Table 7 Continuation results of an invariant torus of the 3D-FHF with respect to ε by using the complete reducibility algorithm: continuation parameter, adjusting parameter, eigenvalues of the linearized equation, angle between bundles and number of Fourier modes

ε	a	λ_2	λ_3	α_{23}	N_F
0.0000000000	3.8832220775	0.0932745366	−1.0721039594	9.13187e−01	64
0.2000000000	3.8651713720	0.0970480228	−1.0318728888	6.67596e−01	64
0.2500000000	3.8596395550	0.0997164626	−1.0054568522	5.80683e−01	64
0.2600000000	3.8584922585	0.1003912484	−0.9989884645	5.61563e−01	64
0.4000000000	3.8413214332	0.1217897138	−0.8282686012	2.07014e−01	64
0.4500000000	3.8348757982	0.1532988873	−0.6598206531	2.99487e−02	64
0.4561361791	3.8340819306	0.1657621720	−0.6104235380	6.03555e−03	512
0.4576004767	3.8338925143	0.1737158508	−0.5825237581	2.60643e−04	131,072
0.4576027468	3.8338922206	0.1737514561	−0.5824044644	2.51665e−04	1,048,576

While the first phenomenon is well understood from classical quasi-periodic bifurcation theory, the second phenomenon is less understood. The number of the Fourier modes increases because the fast and slow stable bundles collide non-uniformly at a parameter

$$\varepsilon_B \simeq 0.45760275,$$

producing the collapse of the algorithm based on reducibility. The failure of the algorithm detects this global phenomenon, in which the reducibility of the torus is lost. Figure 13 reveals the (local) linear behavior with respect to ε of the angle α_{23} between the fast and slow stable bundles (Haro and de la Llave 2006a; Bjerklöv and Saprykina 2008). By fitting α_{23}, we obtain

$$\alpha_{23}(\varepsilon) \simeq 1.78786134 - 3.90637328\ \varepsilon,$$

for $\varepsilon \leq \varepsilon_B$, so that we can extrapolate the critical non-uniform collision value, obtaining

$$\varepsilon_{B,23} \simeq 0.45767806.$$

This bundle merging scenario does not lead to the breakdown of the torus, it only leads to the loss of the reducibility. The phenomenon happens in the stable bundle, which is at positive distance to the tangent bundle along the transition.

In order to avoid the problems caused by the lack of reducibility to a constant cocycle, we use the algorithm based on hyperbolic block-diagonalizability to perform the continuation for ε-values larger than ε_B. The algorithm computes the 2D stable bundle and the corresponding cocycle (Λ_N, R_ω). Then, we compute the Lyapunov multipliers χ_2 and χ_3 and the angle between the corresponding Lyapunov bundles α_{23}, as well as the angle between the tangent and the stable bundle α_{LN}. The results

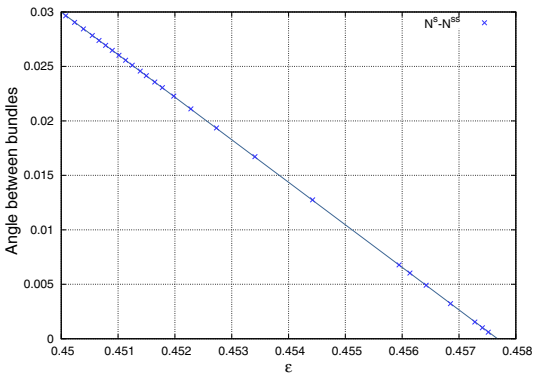

Fig. 13 Continuation results of an invariant torus of the 3D-FHF with respect to ε by using the complete reducibility algorithm: angle between fast and slow stable bundles near the transition at ε_B

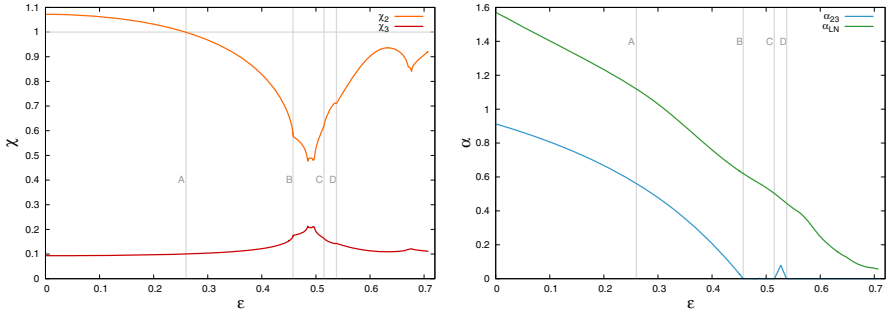

Fig. 14 Continuation results of an invariant torus of the 3D-FHF with respect to ε by using the hyperbolic block-diagonalizability algorithm. *Left* Lyapunov multipliers. *Right* angles between bundles

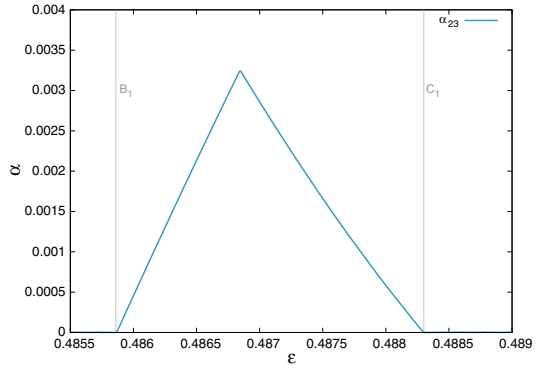

Fig. 15 Continuation results of an invariant torus of the 3D-FHF with respect to ε by using the hyperbolic block-diagonalizability algorithm: magnification of angle α_{23} inside a region between ε_B and ε_C

are summarized in Fig. 14. Besides observing the bundle collision at ε_B, we observe one of the infinitely many gaps in which the fast and slow stable bundles are continuous and the torus is reducible. This main gap takes place between ε_C and ε_D. One tiny gap appears inside the parameter interval [0.485, 0.489], see Fig. 15, between ε_{B_1} and ε_{C_1}.

In these gaps, the torus is reducible of attracting node type, and we can assign a positive or negative sign to the Lyapunov multipliers to obtain the eigenvalues,

Table 8 Continuation results of an invariant torus of the 3D-FHF with respect to ε by using the hyperbolic block-diagonalizability algorithm: continuation parameter, adjusting parameter, eigenvalues of the linearized equation and number of Fourier modes

ε	a	λ_2	λ_3	N_F
0.4000000000	3.8413214332	0.1217898279	-0.8282669115	64
0.4400000000	3.8361693482	0.1423907847	-0.7099672326	64
0.4500000000	3.8348757982	0.1533012145	-0.6598113298	64
0.4600000000	3.8335821637	±0.1766959169	±0.5728158729	64
0.4850000000	3.8303568912	±0.2125670876	±0.4768072652	64
0.4860000000	3.8302283997	-0.2091365623	0.4846543199	64
0.4870000000	3.8300999652	-0.2077106060	0.4880126564	64
0.4880000000	3.8299715897	-0.2076679808	0.4881328051	64
0.4890000000	3.8298432754	±0.2076542462	±0.4881850451	64
0.5000000000	3.8284365048	±0.1919893945	±0.5283807452	64
0.5140000000	3.8266623137	±0.1654852677	±0.6135186826	128
0.5150000000	3.8265364635	-0.1637538925	0.6199920977	128
0.5250000000	3.8252858540	-0.1489775089	0.6819510891	128
0.5300000000	3.8246666229	-0.1451419905	0.7001836965	128
0.5370000000	3.8238076120	-0.1430500564	0.7107233508	128
0.5380000000	3.8236857129	±0.1430877793	±0.7105751874	128
0.6000000000	3.8165452607	±0.1131508954	±0.9020479186	256
0.6501400261	3.8108084316	±0.1105645259	±0.9258623440	4096
0.6708539635	3.8082600966	±0.1192847477	±0.8590492022	8192
0.7001039635	3.8043653898	±0.1130418735	±0.9074951874	8192
0.7071713019	3.8033706211	±0.1113994914	±0.9210259697	1,048,576

In bold it appears the ε parameter values corresponding to pictures in Fig. 16

depending on the action of the cocycle (Λ_N, R_ω) on the corresponding (continuous) Lyapunov bundles. If the numerical method fails to discriminate that the angle α_{23} is strictly positive, we cannot classify the torus as reducible, and we assign $\pm$ to the Lyapunov multipliers. Table 8 displays the results, where the rows in gray represent parameters values where the torus is reducible. A remarkable fact is that, even though the (normal) Lyapunov multipliers do not collide, the signs of the corresponding eigenvalues have been changed in the tiny gap $]\varepsilon_{B_1}, \varepsilon_{C_1}[$, providing new evidences of the lack of reducibility between the gaps. In this example, however, the fast and slow invariant bundles that we have computed in the reducible cases are orientable with index 0.

The continuation slows down when increasing ε, since the number of Fourier modes to get accurate approximations of the invariant tori grows very fast. A view to the invariant tori, see Fig. 16, left, reveals that the torus starts to wrinkle, a phenomenon that has been described as *fractalization route* (Kaneko 1984; Nishikawa and Kaneko 1996) in certain of quasi-periodically forced systems, in the context of strange nonchaotic

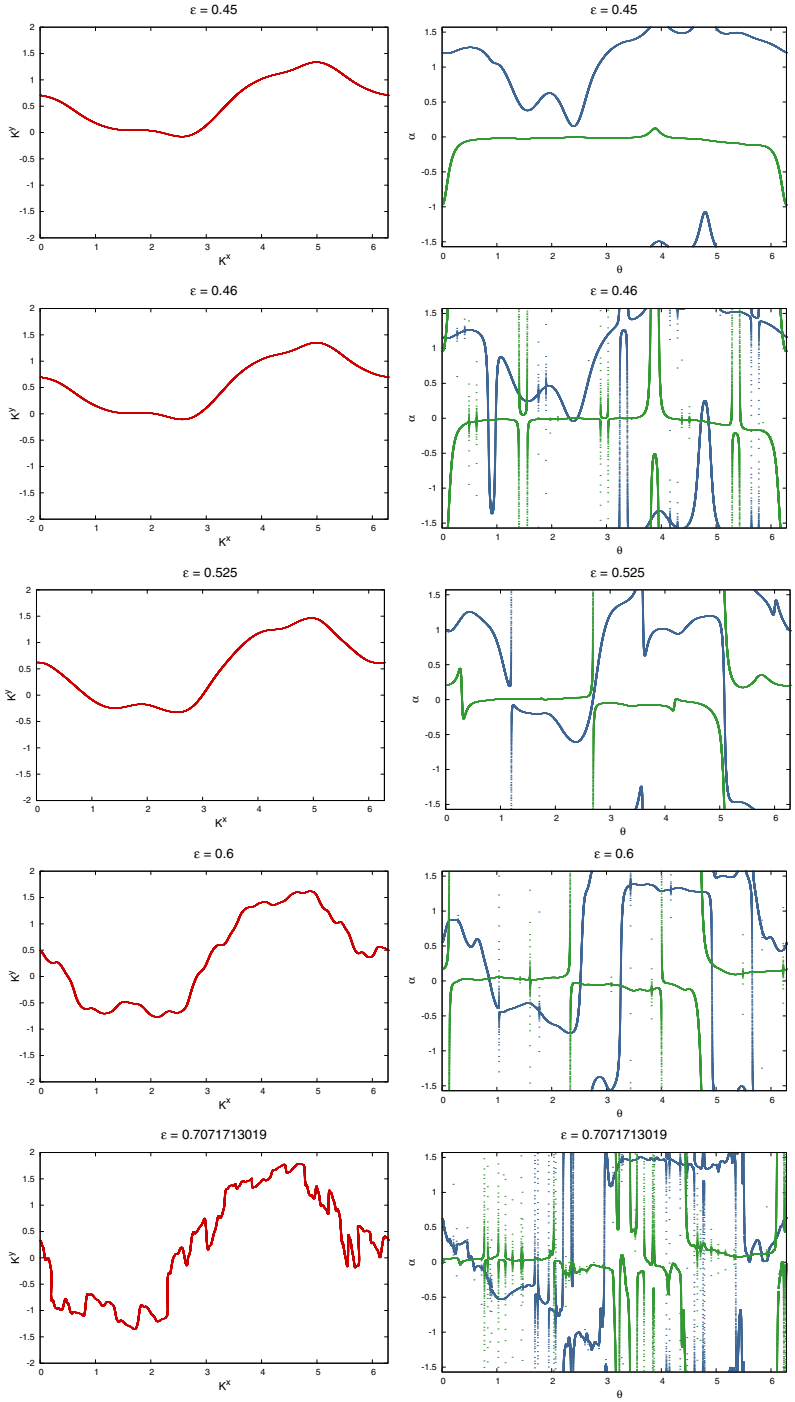

Fig. 16 Continuation of an invariant torus of the 3D-FHF with respect to ε: (x,y)-projection of invariant tori (*left*) and angles of slow and fast bundles with respect to the horizontal axis (*right*)

attractors (Grebogi et al. 1984). A view to the invariant bundles, see Fig. 16, right, adds to this description and explanation (Haro and de la Llave 2006a, 2007): the fact that the torus experiments many reducible/non-reducible transitions (and strange nonchaotic attractors do appear in the projective linearized dynamics) prevents the torus to have a classical smooth bifurcation when the maximal Lyapunov multiplier crosses 1, and produces the destruction of the torus (Haro and Simó 2005). This new fractalization route, and its relation with lack of reducibility, deserves further study.

8 Conclusions

In this paper, we have introduced new numerical techniques for the computation of quasi-periodic normally hyperbolic invariant tori in families of dynamical systems. The algorithms explained here follow the idea of the parameterization method to solve the invariance equation for the invariant torus and the adjusting parameter (and the invariant bundles), and they are well settled in an a posteriori theorem (Canadell and Haro 2016).

The high efficiency of these new numerical methods enables the study of regions in parameter space in which tori are about to break. By monitoring several observables of dynamical and regularity properties, we can detect how hyperbolicity properties degenerate and extrapolate the parameter values in which tori are destroyed. We have presented three mechanisms of breakdown of 1D-tori in families of 3D systems. The examples in Sects. 5 and 6 illustrate two bundle merging scenarios involving the tangent and normal bundle, producing the breakdown of the torus, leading to conjectures 4.1 and 4.4. The example in Sect. 7 presents a new manifestation of a fractalization phenomenon, related to a bundle merging scenario involving the fast and slow stable bundles inside the stable bundle. We hope these numerical results and derived conjectures spur future rigorous studies.

References

Bjerklöv, K., Saprykina, M.: Universal asymptotics in hyperbolicity breakdown. Nonlinearity **21**(3), 557–586 (2008)

Bourgain, J.: On Melnikov's persistency problem. Math. Res. Lett. **4**(4), 445–458 (1997)

Broer, H.W., Huitema, G.B., Takens, F., Braaksma, B.L.J.: Unfoldings and bifurcations of quasi-periodic tori. Memoirs of the American Mathematical Society, vol. 421 (1990)

Broer, H.W., Huitema, G.B., Sevryuk, M.B.: Quasi-periodic motions in families of dynamical systems. Order amidst chaos. Lecture Notes in Mathematics, vol. 1645. Springer, Berlin (1996)

Broer, H.W., Osinga, H.M., Vegter, G.: Algorithms for computing normally hyperbolic invariant manifolds. Z. Angew. Math. Phys. **48**(3), 480–524 (1997)

Cabré, X., Fontich, E., de la Llave, R.: The parameterization method for invariant manifolds. I. Manifolds associated to non-resonant subspaces. Indiana Univ. Math. J. **52**(2), 283–328 (2003)

Calleja, R., Figueras, J.-L.: Collision of invariant bundles of quasi-periodic attractors in the dissipative standard map. Chaos Interdiscip. J. Nonlinear Sci. **22**(3), 033114 (2012). doi:10.1063/1.4737205

Calleja, R., de la Llave, R.: Fast numerical computation of quasi-periodic equilibrium states in 1D statistical mechanics, including twist maps. Nonlinearity **22**(6), 1311–1336 (2009)

Canadell, M.: Computation of normally hyperbolic invariant manifolds. Ph.D. thesis, Departament de Matemàtica Aplicada i analísi, Universitat de Barcelona (2014)

Canadell, M., Haro, A.: Computation of quasi-periodic normally hyperbolic invariant tori: rigorous results. J. Nonlinear Sci. (2016). doi:10.1007/s00332-017-9389-y

Castellà, E., Jorba, À.: On the vertical families of two-dimensional tori near the triangular points of the bicircular problem. Celest. Mech. Dyn. Astron. **76**(1), 35–54 (2000)

Chenciner, A., Iooss, G.: Bifurcations de tores invariants. Arch. Ration. Mech. Anal. **69**(2), 109–198 (1979a)

Chenciner, A., Iooss, G.: Persistance et bifurcation de tores invariants. Arch. Ration. Mech. Anal. **71**(4), 301–306 (1979b)

de la Llave, R., Luque, A.: Differentiability at the tip of Arnold tongues for Diophantine rotations: numerical studies and renormalization group explanations. J. Stat. Phys. **143**(6), 1154–1188 (2011)

Eliasson, L.H.: Almost reducibility of linear quasi-periodic systems. In: Smooth ergodic theory and its applications (Seattle, WA, 1999), volume 69 of Proceedings of Symposia in Pure Mathematics, pp. 679–705. American Mathematical Society, Providence, RI (2001)

Epstein, C.L.: How well does the finite Fourier transform approximate the Fourier transform? Commun. Pure Appl. Math. **58**(10), 1421–1435 (2005)

Figueras, J.-L.: Fiberwise hyperbolic invariant tori in quasiperiodically skew product systems. Ph.D. thesis, Universitat de Barcelona, Barcelona, Spain, May 2011

Figueras, J.L., Haro, A., Luque, A. Rigorous computer-assisted application of KAM theory: a modern approach. Found. Comput. Math. (2016). doi:10.1007/s10208-016-9339-3

Grebogi, C., Ott, E., Pelikan, S., Yorke, J.A.: Strange attractors that are not chaotic. Phys. D **13**(1–2), 261–268 (1984)

Haro, A., Simó, C.: To be or not to be a SNA: that is the question (2005). http://www.maia.ub.es/dsg/2005/0503haro.pdf

Haro, A., de la Llave, R.: Manifolds on the verge of a hyperbolicity breakdown. Chaos **16**(1), 013120 (2006a)

Haro, A., de la Llave, R.: A parameterization method for the computation of invariant tori and their whiskers in quasi-periodic maps: numerical algorithms. Discrete Contin. Dyn. Syst. Ser. B **6**(6), 1261–1300 (2006b)

Haro, A., Puig, J.: Strange nonchaotic attractors in Harper maps. Chaos **16**(3), 033127 (2006)

Haro, A., de la Llave, R.: A parameterization method for the computation of invariant tori and their whiskers in quasi-periodic maps: explorations and mechanisms for the breakdown of hyperbolicity. SIAM J. Appl. Dyn. Syst. **6**(1), 142–207 (2007). **(electronic)**

Haro, A., Canadell, M., Figueras, J.-L.L., Luque, A., Mondelo, J.-M.: The parameterization method for invariant manifolds, volume 195 of Applied Mathematical Sciences. Springer (2016). http://www.springer.com/us/book/9783319296609

Huguet, G., de la Llave, R., Sire, Y.: Fast iteration of cocycles over rotations and computation of hyperbolic bundles. Discrete Contin. Dyn. Syst. S 323–333 (2013). **(Issue special)**

Jalnine, A.Y., Osbaldestin, A.H.: Smooth and nonsmooth dependence of Lyapunov vectors upon the angle variable on a torus in the context of torus-doubling transitions in the quasiperiodically forced Hénon map. Phys. Rev. E (3) **71**(1), 016206 (2005)

Jorba, À.: Numerical computation of the normal behaviour of invariant curves of n-dimensional maps. Nonlinearity **14**(5), 943–976 (2001)

Jorba, À., Simó, C.: On the reducibility of linear differential equations with quasiperiodic coefficients. J. Differ. Equ. **98**(1), 111–124 (1992)

Jorba, À., Simó, C.: On quasi-periodic perturbations of elliptic equilibrium points. SIAM J. Math. Anal. **27**(6), 1704–1737 (1996)

Jorba, À., Tatjer, J.C.: A mechanism for the fractalization of invariant curves in quasi-periodically forced 1-D maps. Discrete Contin. Dyn. Syst. Ser. B **10**(2–3), 537–567 (2008)

Jorba, À., Olmedo, E.: On the computation of reducible invariant tori on a parallel computer. SIAM J. Appl. Dyn. Syst. **8**(4), 1382–1404 (2009)

Jorba, À., Tatjer, J.C., Núñez, C., Obaya, R.: Old and new results on strange nonchaotic attractors. Int. J. Bifurc. Chaos Appl. Sci. Eng. **17**(11), 3895–3928 (2007)

Kaneko, K.: Fractalization of torus. Prog. Theor. Phys. **71**(5), 1112–1115 (1984)

Moser, J.: A rapidly convergent iteration method and non-linear differential equations. II. Ann. Sc. Norm. Sup. Pisa (3) **20**, 499–535 (1966)

Moser, J.: Convergent series expansions for quasi-periodic motions. Math. Ann. **169**, 136–176 (1967)

Nishikawa, T., Kaneko, K.: Fractalization of a torus as a strange nonchaotic attractor. Phys. Rev. E **54**(6), 6114–6124 (1996)

Peckham, B.B., Schilder, F.: Computing Arnol′d tongue scenarios. J. Comput. Phys. **220**(2), 932–951 (2007)
Schilder, F., Osinga, H.M., Vogt, W.: Continuation of quasi-periodic invariant tori. SIAM J. Appl. Dyn. Syst. **4**(3), 459–488 (2005). (electronic)
Sosnovtseva, O., Feudel, U., Kurths, J., Pikovsky, A.: Multiband strange nonchaotic attractors in quasiperiodically forced systems. Phys. Lett. A **218**(3–6), 255–267 (1996)
Vitolo, R., Broer, H., Simó, C.: Quasi-periodic bifurcations of invariant circles in low-dimensional dissipative dynamical systems. Regul. Chaotic Dyn. **16**(1–2), 154–184 (2011)